Theory on Soft X-Ray Magnetic Dichroism of Rare Earth and Transition Metal Compounds

by

Shin Imada

DISSERTATION IN PHYSICS

THE OSAKA UNIVERSITY

GRADUATE SCHOOL OF SCIENCE

TOYONAKA, OSAKA

Theory on Soft X-Ray Magnetic Dichroism of Rare Earth and Transition Metal Compounds

by

Shin Imada

Department of Physics, Faculty of Science

Osaka University

Abstract

A theoretical study of soft X-ray magnetic dichroism, which is a very recently developed field, is carried out for rare earth and transition element ions in typical magnetic states, using an atomic model including intraatomic multiplet interactions. The capability of the magnetic dichroism in probing the magnetic state is shown through clarifying the underlying mechanism and giving interpretations to recently observed spectra.

We first present the calculation of magnetic dichroism in $3d \rightarrow 4f$ and $4d \rightarrow 4f$ X-ray absorption spectroscopies (XAS) of trivalent ions of all rare earth elements under an infinitesimal molecular field on the total angular momentum. The relation between the magnetic dichroism and the $4f$ spin and orbital moment states is clarified in terms of transition operator for photoexcitation by polarized photon, and intraatomic electrostatic and spin-orbit interactions. We also explain the observed magnetic circular dichroism in $3d$ and $4d$ XAS of Gd.

We next calculate the magnetic dichroism in $2p \rightarrow 3d$ XAS of the transition element under a crystalline field and molecular field on the spin, and clarify how the variation in the magnetic state by the applied fields and the $3d$ spin-orbit interaction affects the magnetic dichroism. The spectrum of Co^{2+} ion is shown to reflect the degree to which the $3d$ orbital moment contributes to the total magnetic moment. Furthermore, we demonstrate that the formerly pointed out uniaxial potential on Co^{2+} ion in $CoFe_2O_4$ affects the spectrum considerably,

and interpret the observed magnetic circular dichroism.

Finally, magnetic circular dichroism (MCD) in core X-ray photoemission spectroscopy (XPS), is discussed for both spin-dominant and orbital-moment-dominant ferromagnets. As an example of the former , we choose the $2p$ XPS of a transition element system and give an interpretation to the recent measurement of MCD in $2p$ XPS of Fe. We next discuss, as an example of the latter, the $3d$ XPS of a rare-earth system with $4f^1$ configuration, *i. e.*, Ce^{3+}. Core XPS, especially spin-resolved ones, using circularly polarized beams are furthermore shown to be a promising method to study atomic magnetic states of ferromagnets.

Contents

Charpter I

Introduction

In any spectroscopy using polarized light, the dependence of the spectrum on the polarization of the incident photon can be called dichroism. There are two types of dichroism: linear dichroism is the difference of the spectrum between linearly polarized lights with different planes of polarization; circular dichroism is the difference between two lights with different circular polarizations, namely positive and negative helicities, or left and right circular polarizations. The interaction between polarized light and magnetic substances has attracted much attention since the Faraday effect was found. In the visible light region, dichroism of magnetic materials, or magnetic dichroism, in absorption spectroscopy, together with other magneto-optic effects, has been widely used to investigate the electronic states of magnetic materials.

In this thesis, we focus on magnetic dichroism in core photoabsorption and photoemission spectroscopies using soft X-rays. We aim to clarify from a theoretical aspect the capability of using this phenomenon in probing the microscopic magnetic states by investigating the mechanism by which the magnetic states of rare earth $4f$ and transition element $3d$ orbits are reflected on the magnetic dichroism, and also by giving interpretations to the recently obtained experimental results.

High-energy spectroscopies, *i. e.*, spectroscopies using synchrotron radiation as a main source of photon in the wide energy-range from the visible light

to X-ray, are recently studied intensively, yielding remarkable development in our understandings of electronic, structural and other properties of matters.[1-4] X-ray absorption and X-ray photoemission spectroscopies are among them. In X-ray absorption spectroscopy (XAS), the absorption intensity of X-ray is measured as a function of the photon-energy. In X-ray photoemission spectroscopy (XPS), on the other hand, the intensity of the photoemitted electron is measured as a function of the binding energy, *i. e.,* the difference in energy between the incident photon and the photoelectron.

In XAS, we focus on the spectrum near to the absorption edges in the soft X-ray region, *i. e.,* the photon-energy region from about 50 eV to a few thousand eV, which covers the photoexcitation of electrons from the $2p$ and $3p$ ($3d$ and $4d$) core levels to a $3d$ ($4f$) valence orbit in transition (rare earth) element atoms. In XPS, we focus on core XPS where core electrons are photoemitted again by the soft X-ray. Both spectroscopies can be categorized as core-level spectroscopies.[5-7] The characteristics of core-level spectroscopies are as follows. First of all, one can easily specify the element and its core which is excited. Secondly, multiplet structures in spectra, which are determined by the intraatomic interactions between the photoproduced core hole and the valence electrons of the photoexcited atom, are prominent especially in soft X-ray region. Hence, the spectrum can be a good probe for the state of the valence electrons of the specific element. In solids, the effect of crystalline field or hybridization between the valence orbit and surrounding atomic orbits is often reflected on multiplet structures of spectra. Analyses of various spectra has in fact been carried out and much information about 'solid state effect' has been

extracted.[8-13]

Synchrotron radiation is also making it possible to obtain both linearly and circularly polarized lights in wide energy ranges from vacuum ultraviolet to X-rays. Linearly polarized lights are already obtained in many storage rings. Circularly polarized light has recently become available by using out-of-plane radiation[14,15] or multipole wigglers as insertion devices.[16]

What happens when the incident soft X-ray is polarized? If we consider the selection rule of dipole transition, which is most dominant in the present case, the polarized light gives 'a well-controlled' photoexcitation of core electrons to valence orbits or to the continuum. Magnetic dichroism is well known to arise from the presence of orbital magnetic moment. In core-level spectroscopy, we can fully utilize the strong spin-orbit interaction of the core hole which makes magnetic dichroism also sensitive to the spin moment and also use the multiplet interaction between the core hole and valence electrons, which is sensitive to the distribution of electrons in the $3d$ or $4f$ orbit.[17]

The characteristics of the information extracted from magnetic dichroism of core XAS and XPS can be expected to be as follows:

- It is element-specific.
- The contribution of the spin and orbital moment to the total atomic moment is sensitively and directly reflected on the multiplet structures in the difference spectrum of magnetic circular dichroism or magnetic linear dichroism.
- Magnetic dichroism of various spectroscopies provide information about a given system from various independent viewpoints which are complemen-

tary to each other. This makes the analysis reliable.

Thole *et al.* predicted in 1985 a magnetic linear dichroism (MLD) in $3d$ XAS of rare-earth Dy^{3+} ion.[18] This was followed by an experimental proof by van der Laan *et al.* who measured MLD in $3d$ XAS of an rare-earth Tb in a ferromagnetic TbIG.[19] Goedkoop *et al.* calculated MLD in $3d$ XAS of all rare earth elements.[20] Recently, MLD in $3d$ XAS of Tb[21] and Dy[22] films on Ni and of Dy film on Si[23] were experimentally observed, showing good agreement with the calculations by Thole *et al.*[18] and Goedkoop *et al.*[20] Discussions[18,20] on the relation between the magnetic dichroism and the electronic state has been in terms of total angular momentum of the initial and final states. Although this point of view is in accordance with the ordinary understandings of the magnetic dichroism in the visible light, it does not seem to clarify the characteristics of that in core-level spectroscopy. We should also note that, for systems with net magnetizations as ferromagnets and ferrimagnets, circular dichroism is far more appropriate than linear dichroism in the investigation of magnetic states.

Magnetic circular dichroism (MCD) in XAS was first obtained in the hard X-ray region with photon-energy larger than 5000 eV by Schütz *et al.* who observed MCD in $1s$ XAS of Fe.[24] Since then, MCD in the hard X-ray region has been observed for Fe[25–27] and Ni[26] $1s$ XAS and Pt[28] and rare earths[25,26,29,30] $2p$ and $2s$ XAS in various systems. In these spectroscopies except Pt $2p \rightarrow 5d$ XAS, electric dipole transition($E1$) from the core can reach only extended orbits, and the localized d or f levels are reached only through electric quadrupole transition($E2$). Ebert *et al.* theoretically studied Schütz's results using fully relativistic electronic structure calculation and considering

only $E1$ transition.[28,31–33] Carra *et al.* on the other hand studied MCD in this region considering also $E2$ transition which should contribute to the dichroism reflecting the large polarization in the localized levels.[34,35] When direct information about the magnetic state of $3d$ and $4f$ electrons is sought, MCD in the X-ray region hence does *not* meet the need.

Recently, the first experiment on MCD in the soft X-ray region was carried out by Chen *et al.* in $2p$ XAS of ferromagnetic Ni metal.[14] Sette *et al.* observed MCD in $2p$ XAS of ferromagnetic transition metals and transition elements in ferrites, and in $3d$ XAS of Gd in GdIG.[36] Koide *et al.* observed MCD in Ni $3p$ XAS and in $3p$ XAS of Fe in Fe_3O_4,[15] and Miyahara *et al.* in Ni $3p$ XAS[37] and in Gd $4d$ XAS.[38] For MCD in XPS, MCD in $2p$ XPS of ferromagnetic iron was measured by Baumgarten *et al.* .[39]

Until we calculated MCD in $3d$ and $4d$ XAS of rare earths,[40–43] no study on MCD in XAS in the soft X-ray region, theoretic or experimental, had been done except for studies by Erskine and Stern (1975) who discussed MCD in $3p$ XAS of Ni on the basis of a band model[44] and by Goedkoop *et al.* who pointed out the possibility of application of the MCD to circularly polarization line filters in $3d$ XAS region of some rare earths.[45] Since experimental studies of MCD in soft X-ray region have just started, it seems most desirable for us to systematically investigate the relation between the magnetic states and the magnetic dichroism in core-level spectroscopy in the soft X-ray region, and to clarify its usefulness through analyses of observed data.

For this purpose, we discuss in this thesis, magnetic dichroism in $3d \rightarrow 4f$ and $4d \rightarrow 4f$ XAS of rare earths,[43] $2p \rightarrow 3d$ XAS of transition element[46]

focussing on Co^{2+} in an octahedral symmetry and in $CoFe_2O_4$,[47] $2p$ XPS of transition-element d^8 configuration and $3d$ XPS of rare-earth Ce^{3+} ion.[48,49] As the $3d$ ($4f$) orbital of transition (rare earth) element atoms has a well localized nature even in solids, in this thesis, in order to extract the essential feature of magnetic dichroism, we consider a single magnetic ion. We assume that the ion is in spherical symmetry and under an infinitesimal molecular field on the total angular momentum for rare earths, and in crystalline field and under finite molecular field on the spin for transition element systems.

We should mention that we have also discussed MCD in XAS for mixed-valent Ce compounds, taking into account the hybridization between the $4f$ and conduction band states neglected in this thesis.[40-42] We there showed that an essential feature of MCD can be discussed without the hybridization if the magnetic state is not drastically reformed.

Finally, we note some recent related works. Jo and Sawatzky[50] explained the result obtained by Chen *et al.*[14] taking into account the configuration interaction for Ni 3d state. An analysis of MCD in Ni $2p$ XAS is also carried out by Chen *et al.* .[51] At almost the same time as our studies,[46-49] van der Laan[52] discussed MCD in $2p$ and $3p$ XPS of Cu^{2+}, and van der Laan and B. T. Thole[53] discussed $2p$ XAS of transition elements.

This thesis is organized as follows: In Chapter II, formulations for the calculations of core XAS and core XPS, and their MCD and MLD are given. The mechanisms underlying the emergence of multiplet structures in the spectrum and the reflection of the magnetic state on the magnetic dichroism are presented. In Chapter III, magnetic dichroism in $3d$ and $4d$ XAS of rare earths are

calculated and it is shown that the magnetic state is in fact sensitively reflected on the dichroism. Here, emphasis is placed on MCD. It is also shown that our calculation explains the recently observed MCD in Gd $3d$ and $4d$ XAS very well. In Chapter IV, we discuss the MCD in $2p$ XAS of Co^{2+} whose magnetic state is subject to the crystalline field, spin-orbit coupling and the exchange field. The effect of the formerly pointed out uniaxial potential on the Co in $CoFe_2O_4$ is studied, and an interpretation is given for the recently observed MCD in $2p$ XAS of Co in this system. In Chapter V, MCD in rare-earth $3d$ XPS and transition-element $2p$ XPS is calculated and discussed. We also point out that magnetic dichroism of spin-polarized XPS should be useful for extracting detailed information about the spin and orbital moment states. In Chapter VI, summary is given.

Charpter II

Core-Level Spectra for Polarized X-Rays

In this chapter, we summarize the formulations that will be used in the following chapters.[17] In §1, we prepare the initial and final states of the photoexcitation and the Hamiltonian, which is the source of the multiplet structure in spectra. In §2, a transition operator describing the electron excitation by polarized X-ray is given. We give expressions for dichroism in core XAS and XPS in §3 and §4 respectively and clarify the essential effect of the polarized light.

§1. Initial and final states and Hamiltonian

The system we consider is a single ion in magnetic substances. The ion is in some cases under a crystalline field and/or an molecular field. Its valence orbit is denoted by v: $\mathrm{v} = 3d$ for transition elements, and $\mathrm{v} = 4f$ for rare earths. Let N be the number of the valence electrons. Then, the configuration of the initial state can be written as v^N. $|\mathrm{i}_\alpha\rangle$ with energy E_α is assumed to represent the ground state ($\alpha = 0$) and the excited states ($\alpha \geq 1$). The final states of core XAS and core XPS are assumed to be $\underline{\mathrm{c}}\mathrm{v}^{N+1}$ and $\underline{\mathrm{c}}\mathrm{v}^N + \mathrm{e}^-$ respectively, where $\underline{\mathrm{c}}$ and e^- stand for the photoproduced core hole and the photoemitted electron respectively. We assume that $|\mathrm{f}_\beta\rangle$ denotes the βth final state of the ion having energy E_β, where for XPS, the photoemitted electron is excluded.

The initial and final states are subject to the Hamiltonian

$$H = H_{\mathrm{ee}} + H_{\mathrm{so}} + H_{\mathrm{cr}} + H_{\mathrm{m}}, \tag{2.1}$$

where $H_{\rm ee}$ is the electrostatic interaction between the electrons; $H_{\rm so}$ is the spin-orbit interaction of the valence and core electrons; $H_{\rm cr}$ is the crystal field which is taken into account for transition elements; $H_{\rm m}$ is the molecular field, namely the exchange field on the spin or the infinitesimal molecular field on the total angular momentum, applied in order to produce an atomic magnetic moment.

Since there is at most one core hole, $H_{\rm ee}$ can be written as follows;

$$\begin{aligned} H_{\rm ee} &= \sum_{\xi\xi'}\sum_{\nu\nu'} a_\xi^+ a_\nu^+ a_{\nu'} a_{\xi'} \left(\left\langle \xi\nu \left| \frac{1}{r_{12}} \right| \xi'\nu' \right\rangle - \left\langle \xi\nu \left| \frac{1}{r_{12}} \right| \nu'\xi' \right\rangle \right) \\ &\quad + \frac{1}{2} \sum_{\nu\nu'\lambda\lambda'} a_\nu^+ a_\lambda^+ a_{\lambda'} a_{\nu'} \left\langle \nu\lambda \left| \frac{1}{r_{12}} \right| \nu'\lambda' \right\rangle \\ &= H_{\rm cv}(F_{\rm cv}^k; G_{\rm cv}^k) + H_{\rm vv}(F_{\rm v}^k), \end{aligned} \tag{2.2}$$

where $H_{\rm cv}$ ($H_{\rm vv}$) denotes the interactions between core and valence electrons (between valence electrons) and the definitions of F and G are given later. ξ and ξ' run over one-electron states of the core orbit, and ν, ν', λ and λ' over those of the valence orbit. Thus, the first sum is the interaction between the core and valence, and the second sum is that between the valence electrons. One-electron state is specified by the principal quantum number n, the magnitude and z-component of the orbital moment l and m respectively, and the z-component of the spin σ:

$$|nlm\sigma\rangle = R_{nl}(r) Y_{lm}(\theta\varphi)\psi_\sigma. \tag{2.3}$$

Then the coefficients in $H_{\rm ee}$ is rewritten as

$$\begin{aligned} \left\langle \alpha\beta \left| \frac{1}{r_{12}} \right| \gamma\varepsilon \right\rangle &= \delta(\sigma_\alpha, \sigma_\gamma)\delta(\sigma_\beta, \sigma_\varepsilon)\delta(m_\alpha + m_\beta, m_\gamma + m_\varepsilon) \\ &\quad \times \sum_{k=1}^{\infty} c^k(l_\alpha m_\alpha, l_\gamma m_\gamma) c^k(l_\varepsilon m_\varepsilon, l_\beta m_\beta) R^k(n_\alpha l_\alpha n_\beta l_\beta, n_\gamma n_\gamma n_\varepsilon l_\varepsilon), \end{aligned} \tag{2.4}$$

where $\delta(i,j)$ is one if $i=j$, and zero otherwise. Here, c^k is defined as

$$c^k(lm,l'm') = \sqrt{\frac{4\pi}{2k+1}} \int \mathrm{d}\Omega Y^*_{lm} Y_{k(m-m')} Y_{l'm'}. \tag{2.5}$$

R^k is Slater's integral defined as

$$\begin{aligned} &R^k(n_\alpha l_\alpha n_\beta l_\beta, n_\gamma l_\gamma n_\varepsilon l_\varepsilon) \\ &\quad = \int \mathrm{d}r_1 \mathrm{d}r_2 \frac{r_<^{k+2}}{r_>^{k-1}} R_{n_\alpha l_\alpha}(r_1) R_{n_\beta l_\beta}(r_2) R_{n_\gamma l_\gamma}(r_1) R_{n_\varepsilon l_\varepsilon}(r_2), \end{aligned} \tag{2.6}$$

where $r_<$ ($r_>$) denotes the smaller (larger) of r_1 and r_2. The Slater's integrals we encounter are

$$\begin{aligned} R^k(n_\mathrm{c} l_\mathrm{c} n_\mathrm{v} l_\mathrm{v}, n_\mathrm{c} l_\mathrm{c} n_\mathrm{v} l_\mathrm{v}) &\equiv F^k_\mathrm{cv}, \\ R^k(n_\mathrm{c} l_\mathrm{c} n_\mathrm{v} l_\mathrm{v}, n_\mathrm{v} l_\mathrm{v} n_\mathrm{c} l_\mathrm{c}) &\equiv G^k_\mathrm{cv}, \end{aligned} \tag{2.7}$$

and

$$R^k(n_\mathrm{v} l_\mathrm{v} n_\mathrm{v} l_\mathrm{v}, n_\mathrm{v} l_\mathrm{v} n_\mathrm{v} l_\mathrm{v}) \equiv F^k_\mathrm{v}. \tag{2.8}$$

The values of the Slater's integrals used in this thesis are, in general, obtained by reducing the Hartree-Foch values by 20 to 30%.

The spin-orbit coupling is written as

$$H_\mathrm{so} = \sum_{\xi\xi'} a^+_\xi a_{\xi'} \langle \xi | \zeta_\mathrm{c} \boldsymbol{l} \cdot \boldsymbol{s} | \xi' \rangle + \sum_{\nu\nu'} a^+_\nu a_{\nu'} \langle \nu | \zeta_\mathrm{v} \boldsymbol{l} \cdot \boldsymbol{s} | \nu' \rangle. \tag{2.9}$$

For the parameters ζ's, Hartree-Foch values or experimentally obtained values are used.

Finally, the explicit form of the crystalline field H_cr and the molecular field H_m will be given later in the course of each calculation.

§2. Polarized X-ray

In XAS of transition elements (rare earths) whose $2p$ or $3p$ ($3d$ or $4d$) core electron is excited (hereafter abbreviated as $2p$ XAS or $3p$ XAS ($3d$ XAS or $4d$ XAS) respectively), the electric dipole transition into the $3d$ ($4f$) orbit is dominant to other processes such as electric quadrupole and magnetic dipole transitions. In the case of XPS, it is natural to consider that the core electron is photoemitted to a continuum state with the symmetry which is dipole-allowed, *i. e.,* states with d or s (p or f) symmetries for photoemission in which a $2p$ or $3p$ ($3d$ or $4d$) core electron of transition elements (rare earths) is excited (abbreviated as $2p$ or $3p$ ($3d$ or $4d$) XPS).

Hence, the transition operator that we have to consider is the dipole moment operator $\boldsymbol{E} \cdot \mathbf{r}$, where $\mathbf{r}$ is the position operator for the electron and $\boldsymbol{E}$ represent the electric field of the X-ray. Variation of the electric field with time and position is expressed as $\mathcal{R}\{\boldsymbol{E}e^{i(k\cdot r-\omega t)}\}$, where $\mathcal{R}$ means that the real part is taken.

$\boldsymbol{E}$ for X-ray with an arbitrary polarization has the form

$$\boldsymbol{E} = \mathbf{e}^{(1)}\mathcal{E}^{(1)} + \mathbf{e}^{(2)}\mathcal{E}^{(2)}e^{i\delta}, \tag{2.10}$$

where $\mathbf{e}^{(1)}$ and $\mathbf{e}^{(2)}$ are unit vectors that are perpendicular to each other and are perpendicular to $\mathbf{e}^{(3)}$ which is the unit vector along the wave vector of the X-ray, and three unit vectors have a relation $\mathbf{e}^{(3)} = \mathbf{e}^{(1)} \times \mathbf{e}^{(2)}$. $\mathcal{E}^{(1)}$, $\mathcal{E}^{(2)}$ and δ are real. The polarization of the X-ray is determined by δ. The X-ray has a circular polarization (CP) when $\delta = \pm\frac{\pi}{2}$ and $\mathcal{E}^{(1)} = \mathcal{E}^{(2)}$, and it is said to have positive (negative) helicity when $\delta = +\frac{\pi}{2}(-\frac{\pi}{2})$. When $\delta = 0$, the X-ray has a

linear polarization (LP). Hence, the electric field for CP and LP are expressed as

$$\boldsymbol{E} = \begin{cases} \mathcal{E}(\boldsymbol{e}^{(1)} \pm \boldsymbol{e}^{(2)}) & \text{(CP)} \\ \\ \mathcal{E}\boldsymbol{e} & \text{(LP)} \end{cases} \tag{2.11}$$

where $\boldsymbol{e}$ is in the same plain as $\boldsymbol{e}^{(1)}$ and $\boldsymbol{e}^{(2)}$.

Now, when we calculate magnetic dichroism, we take the z-axis parallel to the magnetic moment. Therefore it is convenient that the transition operator is written in the form

$$\boldsymbol{E} \cdot \boldsymbol{r} = \sum_{\mu=-1}^{1} E_\mu \sqrt{\frac{4\pi}{3}} Y_{1\mu}(\theta\varphi) r, \tag{2.12}$$

where E_μ is defined by

$$\begin{cases} E_{\pm 1} = \dfrac{\mp E_x + \mathrm{i} E_y}{\sqrt{2}} \\ \\ E_0 = E_z \end{cases} . \tag{2.13}$$

For circular polarization, we take $\boldsymbol{e}^{(3)}$ parallel to the z-axis so that E_μ's have the form

$$(E_{-1}, E_0, E_1) = \begin{cases} (0, 0, \mathcal{E}) & \text{(positive helicity)} \\ \\ (\mathcal{E}, 0, 0) & \text{(negative helicity)} \end{cases} . \tag{2.14}$$

Hence positive (negative) helicity can be called 'polarization with $\mu = +1(-1)$.' Linear polarization with $\boldsymbol{E} \parallel z$-axis is expressed as

$$(E_{-1}, E_0, E_1) = (0, \mathcal{E}, 0), \tag{2.15}$$

and corresponds to 'polarization with $\mu = 0$.' That with $\boldsymbol{E}$ which is perpendicular to the z-axis and makes an angle φ to the x-axis is expressed as

$$(E_{-1}, E_0, E_1) = \left(\frac{\varepsilon}{\sqrt{2}} (\cos\varphi + \mathrm{i}\sin\varphi), 0, \frac{\varepsilon}{\sqrt{2}} (\cos\varphi - \mathrm{i}\sin\varphi) \right), \tag{2.16}$$

and is an 'equal superposition of polarizations with $\mu = \pm 1$.'

§3. Core XAS

We define the absorption intensity of X-ray with energy ω by the absorption cross section of an atom:

$$I^{\mathrm{XAS}}(\omega) = \sum_{\alpha} \frac{e^{-\frac{E_{\mathrm{i}\alpha}}{k_{\mathrm{B}}T}}}{Z} \sum_{\beta} \delta(\omega + E_{\mathrm{i}\alpha} - E_{\mathrm{f}\beta}) \frac{\pi\omega \left|\langle \mathrm{f}_\beta \left| \boldsymbol{E}\cdot\mathbf{r} \right| \mathrm{i}_\alpha \rangle\right|^2}{c\varepsilon_0 \boldsymbol{E}^*\cdot\boldsymbol{E}}, \tag{2.17}$$

where $Z = \sum_\alpha e^{-\frac{E_{\mathrm{i}\alpha}}{k_{\mathrm{B}}T}}$ is the partition function for the initial state, and c and ε_0 are the light velocity and the permittivity of vacuum.

The oscillator strength is rewritten as

$$\frac{\pi\omega \left|\langle \mathrm{f}_\beta \left| \boldsymbol{E}\cdot\mathbf{r} \right| \mathrm{i}_\alpha \rangle\right|^2}{c\varepsilon_0 \boldsymbol{E}^*\cdot\boldsymbol{E}} = C^{\mathrm{XAS}}(n_{\mathrm{c}}l_{\mathrm{c}} \to n_{\mathrm{v}}l_{\mathrm{v}}) \frac{1}{\sum_{\mu=-1}^{1} |E_\mu|^2} \left| \sum_{\mu=-1}^{1} E_\mu \left\langle \mathrm{f}_\beta \left| T_\mu^{\mathrm{XAS}}(l_{\mathrm{c}} \to l_{\mathrm{v}}) \right| \mathrm{i}_\alpha \right\rangle \right|^2, \tag{2.18}$$

where

$$C^{\mathrm{XAS}}(n_{\mathrm{c}}l_{\mathrm{c}} \to n_{\mathrm{v}}l_{\mathrm{v}}) = \frac{\pi\omega}{c\varepsilon_0} \left| \int \mathrm{d}r r^3 R^*_{n_{\mathrm{v}}l_{\mathrm{v}}} R_{n_{\mathrm{c}}l_{\mathrm{c}}} \right|^2, \tag{2.19}$$

and

$$T_\mu^{\mathrm{XAS}}(l_{\mathrm{c}} \to l_{\mathrm{v}}) = \sum_{\nu} c^1(l_{\mathrm{v}}m_\nu, l_{\mathrm{c}}m_\xi) a_\nu^+ a_\xi, \tag{2.20}$$

where ξ is determined by a rule

$$\begin{cases} m_\xi = m_\nu - \mu \\ \sigma_\xi = \sigma_\nu \end{cases}; \tag{2.21}$$

a photon with polarization μ increases m of an electron by μ at an excitation. As the width of the range of ω is far smaller than ω itself, we omit the ω dependence (see eq. (2.19)). The square of the coefficient of $a_\nu^+ a_\xi$ in T_μ^{XAS} (see eq. (2.20)), *i. e.*, $|c^1(l_{\mathrm{v}}, m_\nu, l_{\mathrm{c}}(m_\nu - \mu))|^2$, is the magnitude of the transition

$|\xi\rangle \to |\nu\rangle$ by the polarization μ. *The ν- and μ-dependence of this factor is essentially the origin of the polarization dependence of core XAS*; more details will be given in the following chapters.

We can define the absorption intensity for the polarization μ;

$$I_\mu^{\mathrm{XAS}}(\omega) = C^{\mathrm{XAS}}(n_\mathrm{c} l_\mathrm{c} \to n_\mathrm{v} l_\mathrm{v}) \sum_\alpha \frac{e^{-\frac{E_{\mathrm{i}\alpha}}{k_\mathrm{B}T}}}{Z} \sum_\beta \delta(\omega + E_{\mathrm{i}\alpha} - E_{\mathrm{f}\beta}) \left| \left\langle \mathrm{f}_\beta \left| T_\mu^{\mathrm{XAS}}(l_\mathrm{c} \to l_\mathrm{v}) \right| \mathrm{i}_\alpha \right\rangle \right|^2 . \tag{2.22}$$

The absorption of circularly polarized X-ray with positive (negative) helicity is $I_1^{\mathrm{XAS}}(\omega)$ ($I_{-1}^{\mathrm{XAS}}(\omega)$), and circular dichroism is the difference between these two. I_1^{XAS} and I_{-1}^{XAS} will be also denoted by I_+^{XAS} and I_-^{XAS} respectively. The absorption for linear polarization with $\boldsymbol{E} \parallel z$-axis is $I_0^{\mathrm{XAS}}(\omega)$, which shall also be denoted $I_\parallel^{\mathrm{XAS}}(\omega)$. The average of the spectrum for $\boldsymbol{E} \perp z$-axis with respect to the direction of $\boldsymbol{E}$ reduces to $\frac{1}{2}(I_1^{\mathrm{XAS}}(\omega) + I_{-1}^{\mathrm{XAS}}(\omega)) \equiv I_\perp^{\mathrm{XAS}}(\omega)$. We define linear dichroism by the difference between $I_\parallel^{\mathrm{XAS}}$ and $I_\perp^{\mathrm{XAS}}$.

§4. Core XPS

Photoemission spectrum is defined as the intensity of the photoemitted electron as a function of the binding energy $E_\mathrm{B} = \omega - \varepsilon$, where ω and ε are the energy of the photon and the photoelectron. Here, we consider a 'spin resolved core XPS', *i. e.*, the spin of the photoelectron σ is also observed.

Unless the photoemitted core is s level, there are two processes allowed in electric dipole transition, *i. e.*, that increases the magnitude of the orbital moment and that decreases it. Hence, the spectrum $I^{\mathrm{XPS}}(E_\mathrm{B}, \sigma)$, defined by

cross section, can be written as

$$I^{\mathrm{XPS}}(E_{\mathrm{B}},\sigma)=\sum_{\{l=l_{\mathrm{c}}\pm1|l\geq0\}}I^{\mathrm{XPS}}(E_{\mathrm{B}},l\sigma), \tag{2.23}$$

with

$$\begin{aligned}I^{\mathrm{XPS}}(E_{\mathrm{B}},l\sigma)=\sum_{\alpha}\frac{e^{-\frac{E_{\mathrm{i}\alpha}}{k_{\mathrm{B}}T}}}{Z}\sum_{\beta}\delta(E_{\mathrm{B}}+E_{\mathrm{i}\alpha}-E_{\mathrm{f}\beta})\\ \frac{\pi\omega}{c\varepsilon_0\boldsymbol{E}^*\cdot\boldsymbol{E}}\sum_{m=-l}^{l}\left|\langle \mathrm{f}_\beta;\varepsilon lm\sigma\left|\boldsymbol{E}\cdot\mathbf{r}\right|\mathrm{i}_\alpha\rangle\right|^2,\end{aligned} \tag{2.24}$$

where ε should be defined by $\omega-E_{\mathrm{B}}$. $|\mathrm{f}_\beta;\varepsilon lm\sigma\rangle$ denotes the final state including the photoelectron with energy ε, the magnitude and the z-component of orbital moment l and m respectively and spin σ, which is written as

$$|\varepsilon lm\sigma\rangle=R_{\varepsilon l}(r)Y_{lm}(\theta\varphi)\psi_\sigma, \tag{2.25}$$

where the normalization of the radial wave function is given by

$$\int \mathrm{d}r r^2 R_{\varepsilon l}R_{\varepsilon' l}=\delta(\varepsilon-\varepsilon'). \tag{2.26}$$

We rewrite the oscillator strength in the form

$$\begin{aligned}\frac{\pi\omega}{c\varepsilon_0\boldsymbol{E}^*\cdot\boldsymbol{E}}|\langle \mathrm{f}_\beta;\varepsilon lm\sigma|\boldsymbol{E}\cdot\mathbf{r}|\mathrm{i}_\alpha\rangle|^2=C^{\mathrm{XPS}}(n_{\mathrm{c}}l_{\mathrm{c}}\rightarrow\varepsilon l)\\ \frac{1}{\sum_{\mu=-1}^{1}|E_\mu|^2}\left|\sum_{\mu=-1}^{1}E_\mu\sum_{\xi}\delta_{\mu(m-m_\xi)}\delta_{\sigma\sigma_\xi}c^1(lm,l_cm_\xi)\langle \mathrm{f}_\beta|a_\xi|\mathrm{i}_\alpha\rangle\right|^2.\end{aligned} \tag{2.27}$$

The coefficient defined by

$$C^{\mathrm{XPS}}(n_{\mathrm{c}}l_{\mathrm{c}}\rightarrow\varepsilon l)=\frac{\pi\omega}{c\varepsilon_0}\left|\int \mathrm{d}r r^3 R^*_{\varepsilon l}(r)R_{n_{\mathrm{c}}l_{\mathrm{c}}}(r)\right|^2 \tag{2.28}$$

depends on ω, l and ε. We assume that ω and ε is far larger than the width of the range of E_{B} which we consider, so that the coefficient depends only on l and it is denoted by $C^{\mathrm{XPS}}(n_{\mathrm{c}}l_{\mathrm{c}}\rightarrow l)$.

The photoemission intensity by X-ray with polarization μ reduces to

$$I_\mu(E_\mathrm{B}, l\sigma) = C^\mathrm{XPS}(n_\mathrm{c} l_\mathrm{c} \to l) \sum_\alpha \frac{e^{-\frac{E_{\mathrm{i}\alpha}}{k_\mathrm{B}T}}}{Z} \sum_\beta \delta(E_\mathrm{B} + E_{\mathrm{i}\alpha} - E_{\mathrm{f}\beta}) \sum_\xi \delta_{\sigma\sigma_\xi} |c^1(l(m_\xi + \mu), l_\mathrm{c} m_\xi)|^2 \left|\langle \mathrm{f}_\beta \left| a_\xi \right| \mathrm{i}_\alpha \rangle\right|^2 \tag{2.29}$$

Circular and linear dichroism can be defined in the same manner as that in core XAS: we just replace 'XAS' in the last paragraph of §3 by 'XPS.' Finally, as known from eq. (2.29), a photon with polarization μ creates a hole in $|\xi\rangle$ with a probability proportional to $|c^1(l(m_\xi + \mu), l_\mathrm{c} m_\xi)|^2$. *This is the origin of the polarization dependence in core XPS*; more details will be discussed later.

Charpter III

Magnetic Dichroism in XAS of Rare Earths

§1. Introduction

The $4f$ state, which induces the magnetic moment of rare earths, is known to be very well localized even in metallic systems. Furthermore, as the crystalline field of the surrounding atoms is weak compared to the $4f$ spin-orbit interaction, the total angular momentum $\boldsymbol{J}$ is a good quantum number. Hence, an atomic calculation is expected to give a realistic prediction to the experiment. In this chapter, we calculate the magnetic dichroism in $3d$ and $4d$ XAS of all rare earth elements, based on an atomic model in which a trivalent rare earth ion is placed in an infinitesimal molecular field on the total angular momentum. We discuss the mechanism of the magnetic dichroism focussing on MCD, and show that our calculations can give interpretations of the recently observed magnetic circular dichroism in $3d$ and $4d$ XAS of Gd.

$3d$ and $4d$ XAS of rare earths correspond to $d^{10}4f^N \rightarrow d^9 4f^{N+1}$ transitions. In the $3d$ XAS, the strong spin-orbit interaction of the core orbit makes the spectrum split into two peaks corresponding to two values of j of the core hole. Each peak has a multiplet structure of about 10 eV width. As the $4d$ spin-orbit

interaction is weak, $4d$ XAS is not split into two peaks. It has instead a broad and prominent peak called *giant resonance* above the threshold, and in the *prethreshold region*, *i. e.*, the photon-energy range bellow the edge of the giant resonance, it has a multiplet structure which is consisted of weak but sharp peaks. Final states corresponding to the peaks in the prethreshold region are dipole forbidden but for the spin-orbit interaction of the core hole, and have a long life-time of Auger decay. The multiplet structures in the $3d$ and $4d$ XAS, which are determined by the electrostatic interactions of core-$4f$ and $4f$-$4f$, play the roles of fingerprints to identify the $4f$ state.

The characters in the magnetic dichroism depend on whether $3d$ or $4d$ electron is photoexcited. We shall point out the characteristics and discuss the underlying mechanism by considering the effects of transition operator for the polarized X-ray, the spin-orbit interaction of the core hole and the electrostatic interaction between core hole and 4f electrons.

The spin and orbital moment state in the initial state varies according to N, the number of the $4f$ electrons. Therefore, calculation for all rare earths is expected to bring us to a unified picture about what kind of magnetic state causes what kind of dichroism. In our study on MCD of mixed valent Ce compounds, we found that even when the atomic magnetic moment is reduced by the valency mixing, the basic feature of the MCD is conserved unless the property of the spin and orbital moment state is altered thoroughly. Thus, our calculation is also expected to be a good starting point for mixed valent systems.

In §2, we present the calculated result and point out the basic features in

MCD. In §3, we discuss the mechanism of the magnetic dichroism. In §4, we compare the observed MCD in $3d$ and $4d$ XAS of Gd with our calculation and give an interpretation to the experiment. §5 is devoted to conclusions.

§2. Calculated magnetic dichroism

Slater's integrals needed for $d \to 4f$ XAS of rare earths are F_f^2, F_f^4, F_f^6, F_{df}^2, F_{df}^4, G_{df}^1, G_{df}^3 and G_{df}^5, where 'd' stands for $3d$ or $4d$ and 'f' for $4f$. The coefficients for spin-orbit interaction that we need are ζ_d and ζ_f. We show in Table I the adopted values of the Slater's integrals and ζ's. The values for $4f^N$ and $3d^9 4f^{N+1}$ are taken from the paper by Thole et. al.[54] Those for $4d^9 4f^{N+1}$ are taken from the paper by Sugar[55] and for some rare earths, interpolated values are adopted. As the crystalline field is weak compared to the spin-orbit interaction, we assume that $H_{\rm cr} = 0$ (see eq. (2.1)).

The magnetic state in the initial state is determined by assuming zero-temperature and by applying an infinitesimal molecular field parallel to the z-axis, to the total angular momentum of $4f$ electrons:

$$H_{\rm m} = \sum_{\nu} a_\nu^+ a_\nu (-\mu_{\rm B}\mathcal{H}) \langle \nu | J_z | \nu \rangle, \tag{3.1}$$

where $\mathcal{H}$ is positive and infinitesimal. Then the initial state $|{\rm i}\rangle$ is the ground state of $4f^N$ with the lowest J_z: $J = -J_z$.

We show the calculated $3d$ XAS(see Fig. 3.1), $4d$ XAS(see Fig. 3.2) and $4d$ XAS in the prethreshold region (see Fig. 3.3). As functions of the photon energy ω are shown histograms and Lorentzian convolutions with 2Γ = 1.0eV, 2.0eV and 0.2eV for Figs. 3.1, 3.2 and 3.3, respectively. For each element, we show the absorption for positive helicity (I_+) at the top, that for negative helicity (I_-)

at the middle, and that for $\boldsymbol{E} \parallel z$-axis ($I_{\parallel}$) at the bottom. We normalize the spectra by the average of the integrated intensities for the three polarizations. The scale for the histogram is shown at the left, and that for the convoluted curve at the right.

In both $3d$ and $4d$ XAS, character of the MCD is different for $N \leq 5$, $N = 7$ and $N \geq 8$. As $Eu^{3+}(N = 6)$ takes $J = 0$ in the initial state, it shows no dichroism.

In $3d$ XAS(Fig. 3.1), because the spin-orbit interaction of the core hole is strong, the spectra is divided into two parts, corresponding to $3d_{3/2}$ with higher energy(right) and $3d_{5/2}$ with lower energy(left). For $N \leq 5$, the intensity of $3d_{3/2}$ peak for positive helicity is larger than that for negative helicity, while the difference in $3d_{5/2}$ peak is small. The integrated intensity is thus larger in positive helicity than in negative helicity. For Gd^{3+} ($N = 7$), the $3d_{5/2}$ peak is larger in positive helicity than in negative helicity, while the $3d_{3/2}$ peak has the opposite tendency. For $N \geq 8$, the intensity of the $3d_{5/2}$ peak is larger than that of $3d_{3/2}$ in both polarization. The total intensity is larger in positive helicity than in negative helicity, and this tendency is more conspicuous compared to the $N \leq 5$ case.

Next we turn to $4d$ XAS (see Figs. 3.2 and 3.3). For $N \neq 7$, the main peak for positive helicity is in higher energy region than that for negative helicity, and the prethreshold region is larger in negative helicity than in positive helicity. In other words, the whole spectrum is shifted downward in negative helicity compared to positive helicity. For $N \geq 8$, the total intensity is much larger in positive helicity than in negative helicity as in $3d$ XAS. For Gd^{3+} ($N = 7$),

the main peak is shifted about 3eV downward in positive helicity compared to negative helicity.

In addition to the above-mentioned main features, a remarkable dichroism is seen in the fine multiplet structures of $3d_{5/2}$ and $3d_{3/2}$ peaks in $3d$ XAS and and in those of the prethreshold region in $4d$ XAS.

According to the discussion in the preceding chapter, absorption for linearly polarized X-ray with $\boldsymbol{E} \perp z$-axis is the average of those for X-rays with positive and negative helicities. The figures show that although the difference of the total intensity between the two linear polarizations (LP) is smaller than that between two circularly polarized X-rays, linear dichroism is in many cases enhanced by the multiplet interaction of the final state leading to shifts of peaks in different polarization.[18–20)]

§3. Discussion

The goal of this section is to explain how the symmetry breaking of the initial state leads to the main features of MCD. A fundamental factor that connect the symmetry breaking in the initial state and the MCD is of course the transition operator of absorption for each polarization. In $3d$ XAS, we have to consider an additional factor that the spin-orbit interaction is so strong that the total angular momentum of the core hole is nearly a good quantum number. In $4d$ XAS, on the other hand, the electrostatic interaction, particularly the exchange interaction between the core hole and the $4f$ electron, is important.

3. 1 Initial state

According to Hund's rule, the ground state is the LS multiplet with the

largest total spin S, and the largest total orbital moment L allowed under the S. By the spin-orbit interaction, this LS multiplet splits into J multiplets.

When $N \leq 6$, J takes the lowest value $|L - S|$ so that L and S couple antiparallel to each other. As we apply the infinitesimal molecular field along the z-axis, J_z of the initial state is $-J$. When $N \leq 5$, since L is larger than S, the average value of L_z is negative and that of S_z is positive. Hence, *the occupied one-electron states are mainly of up spin and negative m.*

When $N = 7$ (Gd^{3+}), $L = 0$ and $s = 7/2$ so that in the initial state, S_z *is* $-7/2$ *and all the down spin one-electron states are occupied.*

When $N \geq 8$, L and S couple parallel to each other so that $J = L + S$. In the initial state, J_z takes $-J$ and hence the average values of L_z and S_z are both negative so that *the vacant one-electron states are mainly of up spin and positive m.*

3. 2 Transition operator for polarized X-ray

In the present case, the transition operator given in §3, Chapter II is written as

$$T_\mu^{\mathrm{XAS}}(d \to f) = \sum_\nu c^1(3m_\nu, 2m_\xi) a_\nu^+ a_\xi, \tag{3.2}$$

where ξ is determined by ν and μ:

$$\begin{cases} m_\xi = m_\nu - \mu \\ \sigma_\xi = \sigma_\nu \end{cases}. \tag{3.3}$$

In Fig. 3.4, we show the ν- and μ-dependence of $|c^1(3\,m_\nu, 2\,m_\xi)|^2$, the magnitude of the transition $|\xi\rangle \to |\nu\rangle$ by the polarization μ. The figure shows that a polarized X-ray creates a hole-electron pair with a well-defined polarization of

the orbital moment: *in absorption of positive helicity (negative helicity) X-ray, dominant transitions are those into the 4f states with positive (negative) m of larger absolute values.*

This firstly explains the fact that the total absorption of positive helicity is larger than negative helicity apart from Gd^{3+}, for the $4f$ states with positive m are always likelier to be vacant than those with negative m in the initial state for $N \neq 7$ as discussed in the preceding subsection. The differences of the absorptions between the two polarizations are the largest in few elements with the largest N's, where only a few $4f$ states with the largest m's are vacant. In Tm ($N = 12$) there is no intensity for negative helicity($\mu = -1$) because of more rigorous conditions: the initial state has $J = 6$ and the final state configuration can only take $J \leq 6$.

3. 3 3d XAS: the core with strong spin-orbit interaction

$3d$ XAS is one of the cases where the spin-orbit interaction of the core orbit is so large that, in the final state $|\mathrm{f}_\beta\rangle$, the total angular momentum of the core hole j is nearly a good quantum number and takes values $\sim l_\mathrm{c} \pm \frac{1}{2}$. Final states with $j \sim l_\mathrm{c} - \frac{1}{2}\,(l_\mathrm{c} + \frac{1}{2})$ correspond to the higher (lower) photon-energy peak of the two separate peaks. Hence, we replace the (lm) one-electron state of the core by (jj_z) and define the corresponding annihilation operator b_{jj_z}. The transition operator can be separated into two parts creating core holes with different j;

$$T_\mu^{\mathrm{XAS}}(l_\mathrm{c} \rightarrow l_\mathrm{v}) = \sum_{j=l_\mathrm{c}\pm\frac{1}{2}} T_{\mu j}^{\mathrm{XAS}}(l_\mathrm{c} \rightarrow l_\mathrm{v}), \tag{3.4}$$

where

$$T^{\mathrm{XAS}}_{\mu\, l_{\mathrm{c}}+\frac{1}{2}}(l_{\mathrm{c}} \to l_{\mathrm{v}}) = \sum_{\nu} c^{1}(l_{\mathrm{v}} m_{\nu}, l c m_{\xi}) \sqrt{\frac{l_{\mathrm{c}} + 1 + 2\sigma_{\xi} m_{\xi}}{2l_{\mathrm{c}} + 1}}\, a^{+}_{\nu}\, b_{(l_{\mathrm{c}}+\frac{1}{2})(m_{\xi}+\sigma_{\xi})} \quad (3.5)$$

and

$$T^{\mathrm{XAS}}_{\mu\, l_{\mathrm{c}}-\frac{1}{2}}(l_{\mathrm{c}} \to l_{\mathrm{v}}) = \sum_{\nu} c^{1}(l_{\mathrm{v}} m_{\nu}, l c m_{\xi}) \sqrt{\frac{l_{\mathrm{c}} - 2\sigma_{\xi} m_{\xi}}{2l_{\mathrm{c}} + 1}}\, a^{+}_{\nu}\, b_{(l_{\mathrm{c}}-\frac{1}{2})(m_{\xi}+\sigma_{\xi})}. \quad (3.6)$$

Using $T_{\mu j}$, the absorption intensity can be approximated as

$$I^{\mathrm{XAS}}_{\mu}(\omega) \approx I^{\mathrm{XAS}}_{\mu l_{\mathrm{c}}+\frac{1}{2}} + I^{\mathrm{XAS}}_{\mu l_{\mathrm{c}}+\frac{1}{2}}, \quad (3.7)$$

where

$$I^{\mathrm{XAS}}_{\mu l_{\mathrm{c}} \pm \frac{1}{2}} = C^{\mathrm{XAS}}(n_{\mathrm{c}} l_{\mathrm{c}} \to n_{\mathrm{v}} l_{\mathrm{v}}) \sum_{\alpha} \frac{e^{-\frac{E_{\mathrm{i}\alpha}}{k_{\mathrm{B}} T}}}{Z} \sum_{\{\beta | j \sim l_{\mathrm{c}} \pm \frac{1}{2}\}} \delta(\omega + E_{\mathrm{i}\alpha} - E_{\mathrm{f}\beta}) \left| \left\langle \mathrm{f}_{\beta} \left| T^{\mathrm{XAS}}_{\mu l_{\mathrm{c}} \pm \frac{1}{2}}(l_{\mathrm{c}} \to l_{\mathrm{v}}) \right| \mathrm{i}_{\alpha} \right\rangle \right|^{2}. \quad (3.8)$$

In Fig. 3.5, we show the magnitudes of the transition to $|\nu\rangle$ in the operator $T^{\mathrm{XAS}}_{\mu j}$ corresponding to the peak d_j. This shows that when the core level has a large spin-orbit interaction, a polarized X-ray creates a hole-electron pair with well defined polarization of spin and orbital moment: *in photoabsorption creating the 3d hole with $j = 5/2$ $(3/2)$, dominant transitions are those into the 4f states whose m and spin are of the same (opposite) sign.* This readily shows that $3d$ XAS can be a probe for the relation of the orientations of L and S in the initial state.

We can qualitatively explain the main feature of MCD in $3d$ XAS discussed in §2, by comparing the dominant transitions with the mainly vacant $4f$ state in the initial state (see 3.1 and Fig. 3.5).

For elements with $N \leq 5$, transitions with the largest weights are allowed except in $T_{-1,3/2}$, since in the initial state the $4f$ electrons are mainly in the orbits with up spin and negative m. This explains the fact that the intensity of $3d_{5/2}$ peak is about the same in positive helicity and negative helicity and that of $3d_{3/2}$ is smaller in negative helicity than in positive helicity.

For Gd^{3+} ($N = 7$), since all the up spin $4f$ orbits are completely unoccupied in the initial state (see 3.1), dominant transitions are allowed in $T_{+1,5/2}$ and in $T_{-1,3/2}$, which explains the fact that the $3d_{5/2}$ ($3d_{3/2}$) peak is larger in positive helicity (negative helicity).

For elements with $N \geq 8$, dominant transitions are allowed only in $T_{+1,5/2}$, since the $4f$ orbits vacant in the initial state are mainly those with up spin and positive m. This explains the fact that only the $3d_{5/2}$ peak in positive helicity is strong. The magnitudes of other peaks also qualitatively agrees the total weight of the allowed transitions.

3. 4 4d XAS: the core with weak spin-orbit interaction

In order to interpret the characters found in MCD of $4d$ XAS, we have to consider the electrostatic interaction between the core hole and the $4f$ electrons. This factor plays a dominant role in determining the energies of the main peaks for each polarization of the X-ray. The spin-orbit interaction of the $4d$ hole is weak so that it does not affect the spectrum very much, except in Gd^{3+} for which the dichroism is entirely due to the spin-orbit interaction of the $4d$ core hole because $L = 0$ in the initial state.

The energy of the main peak is expressed approximately as

$$\frac{\langle \mathrm{f}_0|H|\mathrm{f}_0\rangle}{\langle \mathrm{f}_0|\mathrm{f}_0\rangle}, \tag{3.9}$$

where $|\mathrm{f}_0\rangle = T_\mu|\mathrm{i}\rangle$. The most important term in H (see eq. (2.1)) is H_{ee}, particularly, the $k = 1$ term in the exchange interaction in H_{cv}, namely

$$-\sum_{\xi\xi'}\sum_{\nu\nu'} a_\xi^+ a_\nu^+ a_{\nu'} a_{\xi'} \left\langle \xi\nu \left| \frac{1}{r_{12}} \right| \nu'\xi' \right\rangle_1, \tag{3.10}$$

where

$$\begin{aligned}\left\langle \xi\nu \left| \frac{1}{r_{12}} \right| \nu'\xi' \right\rangle_1 =& \delta(\sigma_\xi, \sigma'_\nu)\delta(\sigma_\nu, \sigma'_\xi)\delta(m_\xi + m_\nu, m'_\nu + m'_\xi) \\ & c^1(l_{\mathrm{c}} m_\xi, l_{\mathrm{v}} m'_\nu) c^1(l_{\mathrm{c}} m'_\xi, l_{\mathrm{v}} m_\nu) G^1_{df}\end{aligned} \tag{3.11}$$

We can explain the difference of the main peak energies between the two polarizations except for Gd^{3+}, keeping in mind the following three facts. a) The exchange interaction between the core hole and the $4f$ electron lifts up the energy of the final state. b) The exchange interaction between a core hole and an excited $4f$ electron is proportional to the weight of the corresponding transition(see Fig. 3.4) because they are both determined by the same c^1's (see eqs. (3.11) and (2.20)). c) A core hole has the exchange interaction only with a $4f$ electron with the same spin as the photoexcited electron(see eq. (3.11)).

3. 4. 1 $n \leq 5$.

The dominant excitations allowed by the positive helicity X-ray are those into the $4f$ states with the highest m's and both spins, and for the negative helicity the $4f$ states with the lowest m's and down spin, since the $4f$ states with negative m and up spin are mainly occupied in the initial state. The fact b) is

irrelevant to the present MCD, for the weights of the allowed dominant transitions are about the same for both polarizations. In positive helicity, because electrons of both spins are excited, the core hole can have exchange interactions not only with the excited electron but also with the preexisting $4f$ electrons. On the other hand, in negative helicity, because electrons mainly of down spin are excited, the core hole can have exchange interactions only with the excited electron. The energy of the main peak in positive helicity is thus higher than that in negative helicity because of the fact c), if we note the fact a).

3. 4. 2 $n \geq 8$.

Excitations allowed are those into the vacant $4f$ states with mainly positive m and up spin in both polarizations. The fact c) is irrelevant to the present MCD, for the spin of an excited electron is the same in both polarizations. The fact a) and b) tells us that the contribution of the exchange interaction between the core hole and the excited electron is larger in positive helicity than in negative helicity because the weights of the allowed transitions are larger in positive helicity (see 3.2 and Fig. 3.4). This is the reason why the energy of the main peak is higher in positive helicity than in negative helicity.

3. 4. 3 prethreshold region

Throughout $1 \leq n \leq 5$ and $8 \leq n \leq 12$, the spectral intensity of the prethreshold region is weaker for positive helicity than for negative helicity. This can be understood as follows. The lines in this region are induced from those in the giant resonance through the spin-orbit interaction. Therefore, they are stronger in negative helicity whose giant resonance is located at lower

photon-energy, *i. e.*, nearer to the prethreshold region.

§4. Comparison with experiments

Sette *et al.*[36] and Miyahara *et al.*[38] have recently observed MCD in Gd $3d$ XAS in $Fe_5Gd_3O_{12}$ (GdIG) and Gd $4d$ XAS in ferromagnetic Gd metal, respectively. In this section, we give an interpretation to their spectra by comparing them with our calculations.

GdIG is one of the rare-earth iron garnets (RIG), and is a ferrimagnet with a garnet structure: Fe^{3+} ions are distributed in two sites (a- and d-site) and magnetic moments of a- and d-site couple antiferromagnetically; Gd^{3+} ion couples antiparallel to Fe in the d-site.

In Figs. 3.6 and 3.7, we show the calculated spectra at the top and the experimental result at the bottom for $3d$ XAS and prethreshold region of $4d$ XAS.

The observed MCD ('positive' minus 'negative' helicity) of $3d$ XAS (see Fig. 3.6) is positive in $3d_{5/2}$ peak and is negative in $3d_{3/2}$, in agreement with our calculation. This shows that, the magnetic moment of the Gd^{3+} ion in GdIG is completely arises from its spin(see 4. 3). Furthermore, multiplet structure in the calculated MCD is well reproduced in the experiment: structures labeled A-C corresponds to a-c, and structures D and E leads to the asymmetry labeled d and e. In $4d$ XAS, too, agreement between the calculated and experimental MCD is excellent except for some discrepancies: structures labeled A-F corresponds to a-f; structures G and H seems to be canceled out. Thus, we can conclude that in our calculation are reproduced very well the atomic magnetic state and the

excitation process of $3d$ and $4d$ XAS by polarized X-rays, in the actual systems.

The intensity of the MCD is smaller in the experiment than in the calculation. One cause for this is the imperfectness of the circularity of the X-ray: (*e. g.* Sette *et al.* reported that their circularity was calculated to be $85\% \pm 10\%$). The other cause is expected to be that the sample is not saturated, *i. e.*, there are magnetic domains having different orientations of magnetic moment.

We finally compare the average of the observed spectra for 'positive' and 'negative' helicities with the calculation. Even if the circularity of the circularly polarized X-ray is imperfect, when the sample is saturated, the sum of the 'positive' and 'negative' helicity must correspond perfectly to the calculated $(I_+ + I_-)/2$, *i. e.*, $I_\perp$. However, both in $3d$ and $4d$ XAS, the observed average spectrum is reproduced better by the calculated absorption of unpolarized X-rays ($(I_+ + I_- + I_\parallel)/3$) than by $I_\perp$. This is explained by assuming that the magnetization of the sample is very small because of domain-formation.

§5. Conclusion

We calculated the MCD in $3d$ and $4d$ XAS of all rare earth elements assuming trivalency, pointed out the features of the dichroism, and explained the origin by an intuitive discussion. The observed MCD in $3d$ and $4d$ XAS of Gd was interpreted by comparing them with the calculated result.

The main property of MCD in $3d$ XAS appeared in the magnitudes of $3d_{3/2}$ and $3d_{5/2}$ peaks. The magnitude of each peak was shown to reflect the total weight of the corresponding transitions allowed by the spin and orbital moment occupation, *i. e.*, the contribution of the spin and orbital moment to

$4f$ moment, in the initial state.

The character of $4d$ XAS was found in the imbalance of the whole intensity between the polarizations, in the energy shift of the main peak, and as a consequent of this, in the difference in the strength of the prethreshold structure. The imbalance of the whole intensity was found to reflect the population of the orbital moment. The energy shift was explained by the difference in the exchange interaction between the core hole and $4f$ electrons in the final state yielded by each polarization.

The symmetry breaking of the initial state is thus sensitively reflected to the dichroism through the difference of the transition operator between polarizations, the spin-orbit interaction of the core hole ($3d$ XAS) and the exchange interaction ($4d$ XAS) in the final state. $3d$ and $4d$ XAS are complementary to each other in investigation of the symmetry breaking in rare earth magnetic systems.

Circular dichroism of multiplet structures were seen in both $3d$ and $4d$ XAS. This is very useful in studying the variation of mixed valency and symmetry breaking of the initial state caused by hybridization between valence electrons and conduction or valence band and by a crystalline field. We note that the fine structures in the prethreshold region of the $4d$ XAS must be especially sensitive to the variation.

Finally, we applied our calculation for interpretation of the recently observed MCD in $3d$ and $4d$ XAS of Gd in GdIG and Gd metal respectively. The signs of $3d_{5/2}$ and $3d_{3/2}$ peaks in the observed MCD in $3d$ XAS of Gd was interpreted as a typical character for atomic magnetic moment dominantly in-

duced by spin. The MCD in the experimental $3d$ and $4d$ XAS showed multiplet structures that reproduces the calculation very well except for some discrepancies. The average of the observed XAS by circularly polarized X-rays showed good agreement with the calculated XAS by unpolarized X-ray, which indicates that the sample is not magnetically saturated. Hence, we proved the validity of our calculation and the usefulness of MCD as a tool to investigate the atomic magnetic state.[43)]

Charpter IV

Magnetic Dichroism in XAS of Transition Elements

§1. Introduction

The various electronic and magnetic states of $3d$ electrons in magnetic materials have been and still are objects of researches. It is therefore necessary for us to know what contribution the magnetic dichroism in XAS, the newly developed tool, can make to the study of this field. In this chapter, we discuss particularly what information about ionic magnetic materials the magnetic circular dichroism in $2p \rightarrow 3d$ XAS can reveal. A characteristic thing about this spectrum is that, because $2p$ orbit has a strong spin-orbit interaction, the spectrum is separated into two parts, namely $2p_{3/2}$ and $2p_{1/2}$, corresponding to $3d \rightarrow 4f$ XAS of rare earths.

Recently, Chen *et al.*[14] and Sette *et al.*[36] observed MCD in $2p$ XAS of transition elements in ferromagnetic metals and ionic insulators. MCD for metallic substances, in which the $3d$ electrons are itinerant, was shown to reflect the spin and orbital moment state of configuration-mixed $3d$ state.[50] In ionic materials, magnetic states constructed of the localized $3d$ electrons are diverse because the electrons are subject to a strong crystalline field, an exchange field on the spin and a spin-orbit interaction. This is in quite contrast

with $4f$ magnetic state in rare earths. The aim of this chapter is to show that the MCD in $2p$ XAS can be a good tool for specifying what magnetic state is realized. We choose the MCD of $2p$ XAS of Co as an example. We show in §2, that from the MCD, we can estimate the amount of the orbital moment, which, because of the strong crystalline field, should be zero if spin-orbit interaction is neglected. We then discuss in §3, how the MCD reflects the effect of the uniaxial potential acting on Co^{2+} ion in $CoFe_2O_4$, which was formerly pointed out to be important,[56,57] and also give an interpretation to the observed MCD. This discussion gives evidence that a detailed information can be extracted from the MCD. In §4 is given a concluding remark.

§2. Magnetic dichroism in $2p$ XAS

$3d$ electrons of transition element ion in ionic material are subject to a strong crystalline field $H_{\rm cr}$ produced by the surrounding ions. Although $H_{\rm cr}$ is weaker than the intraatomic electrostatic interaction $H_{\rm ee}$, it is stronger than the spin-orbit interaction $H_{\rm so}$ and the molecular field $H_{\rm m}$. The molecular field is consisted of exchange or superexchange interaction between the $3d$ electron and the valence electrons of neighboring magnetic ions, and is assumed to be applied on the spin. If we assume that $H_{\rm so} = 0$, in the magnetic state induced by $H_{\rm m}$, the orbital moment is quenched and the magnetic moment is made only of spin moment, *i. e.*, $\langle \boldsymbol{l} \rangle = 0$. But if we consider $H_{\rm so} \neq 0$, except in the case where the L determined by the Hund's rule is zero, the orbital moment is not completely quenched. The extent to which the strength of the orbital moment recovers is determined by the interplay of all the terms in the Hamiltonian.

In this section, we show that the MCD can be a good tool in estimating the magnitude of the orbital moment. We take $2p \rightarrow 3d$ XAS of Co^{2+} as an example and compare the MCD for some typical Hamiltonians. We assume that the ion is placed in an octahedral crystalline field:

$$H_{\rm cr} = \frac{105Dq}{2r^4}\left(x^4 + y^4 + z^4 - \frac{3}{5}r^4\right) \equiv V_{\rm c}. \tag{4.1}$$

The molecular field applied on the $3d$ spin is assumed as

$$H_{\rm m} = \sum_{\nu} a_{\nu}^{+} a_{\nu} 2\mu_{\rm B}\mathcal{H}\langle\nu|\sigma|\nu\rangle. \tag{4.2}$$

where $\mu_{\rm B}\mathcal{H}$ is assumed to be 0.1eV in this section. Slater's integrals in $H_{\rm ee}$ (see eq. (2.2)) and ζ's in $H_{\rm so}$ (see eq. (2.9)) are assumed as follows:[58] for the initial state, $F_d^2 = 9.28$, $F_d^4 = 5.77$, and we vary the values of $10Dq$ and ζ_d; for the final state, $F_{pd}^2 = 5.81$, $G_{pd}^1 = 4.32$, $G_{pd}^3 = 2.46$, $F_d^2 = 9.92$, $F_d^4 = 6.17$, $\zeta_d = 0.083$, and $\zeta_p = 9.75$.

In Fig. 4.1, we show the calculated $2p$ XAS of Co^{2+} ion for circularly polarized X-rays: total spectrum $((I_+ + I_-)/2)$ at the top, and the MCD $((I_- - I_+)/2)$ at the bottom. In the left column, $10Dq = 1.2$eV and $\zeta_d = 0$ leading $\langle m\rangle = 0$ and $\langle\sigma\rangle = -1.5$. The MCD feature in this case is explained as follows. Because the $3d$ occupation is symmetric with respect to an operation $m \rightarrow -m$, the integrated absorption intensity is the same for both circular polarizations (see Fig 4.2). Thus, the integrated MCD is zero. In $2p_j \rightarrow 3d$ absorption by circular polarization, the weights of transitions to $3d$ states are distributed as shown in Fig. 4.3. As the holes are only in the $\sigma > 0$ states, $d_{3/2}$ ($d_{1/2}$) peak is larger for positive (negative) helicity, which leads to the MCD pattern.

In the center column, $10Dq = 1.2$eV and $\zeta_d = 0.066$eV leading $\langle m \rangle = -1.59$ and $\langle \sigma \rangle = -1.48$. As $\langle m \rangle < 0$, *i. e.,* holes are more likely to be found in $m > 0$, $I_{+1\,3/2}$ is enhanced and $I_{-1\,1/2}$ is suppressed while effects on other peak intensities are small, making the $d_{3/2}$ peak in MCD grow and $d_{1/2}$ peak shrink.

In the right column, $10Dq = 0$ and $\zeta_d = 0.066$eV leading $\langle m \rangle = -3.0$ and $\langle \sigma \rangle = -1.5$. Although this condition is not realistic for transition elements in solids, we show the spectrum for comparison. As the $3d$ state is now similar to the $4f$ state of the more-than-half-filled case ($N \geq 8$) in rare earths, the spectra also show resemblance if we replace the $2p_{3/2}$ and $2p_{1/2}$ by $3d_{5/2}$ and $3d_{3/2}$ respectively.

§3. MCD in $2p$ XAS of Co in $CoFe_2O_4$

In the light of our discussion in the previous section, the MCD in $2p$ XAS of Co in $CoFe_2O_4$, which was recently observed by Sette *et al.*[36], shows that the orbital moment of Co^{2+} is rather large. Furthermore, Slonczewski and Tachiki pointed out, in their studies on the magnetic anisotropy of $CoFe_2O_4$,[56,57] that not only the spin-orbit interaction but also a uniaxial potential plays an important role in determining the $3d$ state of the Co. In this section, as a test of the capability of the MCD, we examine how sensitively the MCD in $2p$ XAS reflects the modification of the electronic state by the uniaxial potential.

3. 1. Trigonal potential on Co in $CoFe_2O_4$

$CoFe_2O_4$ is a ferrimagnet with Curie temperature $T_C = 520°C$.[59] It has the inverse spinel structure, namely, Co^{2+} ions are in the octahedral sites (B sites), where they are surrounded octahedrally by O^{2-}, half of the Fe^{3+} ions

are in B sites and the other half are in the tetrahedral sites (A sites). In the ferrimagnetic state, magnetic moments of ions in the $B(A)$ sites are parallel (antiparallel) with the total magnetization. If we neglect the difference in the species of cations, each B site lies on an axis of threefold symmetry which is parallel to one of the body diagonals of the cubic crystal. This symmetry is illustrated in Fig. 4.4. B sites may be classified into four kinds, each lying on one of the four trigonal axes (1 1 1, $\bar{1}$ 1 1, 1 $\bar{1}$ 1, $\bar{1}$ $\bar{1}$ 1). The easy axes are the three axes equivalent with [001] axis

In the cubic crystalline field, the ground level of a free Co^{2+} ion (^4F) splits into three orbital levels, namely Γ_4, Γ_5 and Γ_2, and the lowest is the triplet Γ_4. This lowest level splits into a doublet and a singlet by the trigonal field due to the averaged charge distribution of the ions in the B sites, Fe^{3+} ions in the A sites and the oxygen ions slightly distorted from the octahedral arrangement. It is assumed that the doublet lies lower. When we take into account the spin-orbit interaction and the molecular field on the spin, these doublet and singlet are mixed again to yield the ground state. The cubic crystalline field is of the order of $\sim$ 1eV, and the trigonal field, the spin-orbit interaction and the molecular field on spin are all of the same order, $\sim$ 0.1eV. Although there is a site-dependent crystalline field of a lower symmetry arising from a certain arrangement of Fe^{3+} and Co^{2+} around the center Co^{2+}, this field is assumed to be of a still smaller magnitude[56,57] ($\sim$ 0.01eV) and will be neglected in the present discussion.

3. 2. Trigonal field and temperature-dependent MCD

We assume that the additional uniaxial field, which along with the cubic

field makes the whole field trigonal, is of the lowest order:

$$V_{\rm t} = -\frac{2p}{r^2}(xy + yz + zx). \tag{4.3}$$

In Fig. 4.5(a)-(d), we show the calculated total XAS ($(I_+ + I_-)/2$) and MCD ($(I_- - I_+)/2$) in temperatures $T = 0$ and 300K for a cubic field ($10Dq = 1.2$eV and $p = 0$) and for a trigonal field ($10Dq = 1.2$eV and $p = 0.3$eV: this corresponds to the magnitude of the trigonal field assumed by Slonczewski[56]). ω here represents the relative photon energy. The $10Dq$ of the cubic field was determined so that the total XAS reproduces the observed one. Values for Slater's integral and the ζ's are the same as in the previous section, except for $\zeta_d = 0.033$eV in the initial state, which is also assumed after Slonczewski.[56] As the easy axes are the three axes equivalent with [001] axis, we apply the molecular field along the z-axis (see eq. (4.2)). $\mu_{\rm B}\mathcal{H} = 0.035$eV is assumed at $T = 300$K. At $T = 0$, although $\mu_{\rm B}\mathcal{H}$ should be larger to some extent, we adopt the same value as at $T = 300$K because the effect of the variation of $\mu_{\rm B}\mathcal{H}$ around 0.035eV on the electronic state is negligible.

At the zero temperature (see Figs. 4.5 (a) and (b)), both the total XAS and MCD are clearly affected by the trigonal crystalline field. The effect is that peaks B and D decrease compared with peaks A and C respectively. The difference comes from the change in the direction of the orbital moment in the ground state: the trigonal crystalline field makes the orbital moment cant along the direction of the trigonal axis. The integrated MCD, a quantity closely related to the m state, are approximately $-3/4$ and $-1/2$ times the integrated total XAS for $p = 0$ and 0.3, reflecting $\langle m \rangle = -1.46$ and -0.98 respectively.

At 300K(see Figs. 4.5 (c) and (d)), the effect of the trigonal crystalline field on the spectral shape is smaller both in the total XAS and in the MCD. The integrated MCD is approximately $-3/8$ and $-1/4$ times the integrated total XAS for $p = 0$ and 0.3 reflecting $\langle m \rangle = -0.78$ and -0.54, respectively.

Our calculation predicts that the effect of the trigonal crystalline field, if exists, will be reflected in the MCD spectrum at low temperatures. Temperature dependence of not only the spectral shape of the MCD but also the integrated MCD is expected to be useful in studying solid state effects on electronic state of magnetic ion.

In figs. 4.5 (e) and (f), we show the experimental result of $2p$ XAS and its MCD obtained at the room temperature by Sette *et. al.*[36]. Our calculation for $T = 300$K with both $p = 0$ and 0.3 agree with the experiment well. For $p = 0$ (0.3) the calculated spin and orbital moment contributions to the magnetic moment of Co^{2+} are $2.80(2.84)\mu_B$ and $0.78(0.54)\mu_B$ respectively.

§4. Conclusion

The MCD in $2p$ XAS of transition elements was shown to depend sensitively on the spin and orbital moment contribution to the magnetic state of $3d$ electrons, which is deformed by the interplay of the crystalline field, the molecular field and the spin-orbit interaction, using transition element Co^{2+} ion as an example. To show that MCD can be used to determine the electronic and magnetic state in detail, we predicted the effect of trigonal crystalline field expected on the spectrum at low temperatures in $CoFe_2O_4$. The MCD can thus be used to *observe* the strength of the trigonal field, which has not been done yet. We also

explained the observed MCD in Co $2p$ XAS.[47)]

Charpter V

Magnetic Dichroism in Core XPS

§1. Introduction

The measurement of MCD in the $2p$-core x-ray photoemission ($2p$ XPS) has been recently made by Baumgarten *et al.* in ferromagnetic Fe.[39] Although an explanation with use of a phenomenologically introduced core-valence exchange interaction is given to the observed feature of MCD in Fe $2p$ XPS,[39] discussions seem to be still controversial and a unified picture to clarify the MCD feature is absent for the $2p$ XPS in transition-element systems and the $3d$ XPS in rare-earth systems. It should be noted that the phenomenological exchange interaction cannot distinguish whether the atomic magnetic moment arises from spin or orbital moment.

The purpose of this chapter is to discuss theoretically a basic MCD feature in $2p$ XPS in ferromagnetic transition-element systems and $3d$ XPS in rare-earth systems. For core XAS spectra, it has been shown that an essential feature of MCD calculated by using an atomic model is maintained even in solids such as Ni[50] and Ce,[40–42] even if modified to some extent by 'solid state effect' such as hybridization. The present approach for XPS neglecting the hybridization between the $3d$ or $4f$ orbital of an atom in question and surrounding 'delocalized' orbits is at least expected to be a starting point for

our purpose. We first discuss the MCD in $2p$ XPS for an atom with $3d^8$ under a crystalline and a molecular field as an example of spin-dominant ferromagnets such as Fe. Our calculation will show that the observed basic feature of MCD in Fe $2p$ XPS is common to the case where the $2p \rightarrow d$ transition is dominant compared with the $2p \rightarrow s$ and the $3d$ spin mainly contributes to an atomic magnetic moment. Next we discuss the MCD in $3d$ XPS for an atom with $4f^1$ under an infinitesimal molecular field on the total angular momentum as an example of the orbital-moment-dominant ferromagnet seen in many rare-earth systems. We will see that the MCD feature in XPS is basically determined by the direction of spin moment in the valence electron system, the selection rule of the photoexcitation and the exchange interactions between valence electrons and a photo-produced core-hole in the final state of the photoemission.

§2. Spin-dominant magnetic state

We first give an intuitive discussion about the MCD in $2p$ XPS for $3d$ atoms where the $3d$ spin contributes to an atomic magnetic moment (see Fig. 5.1) and then present calculated results for the spin-polarized initial state with $3d^8$ configuration (see Fig. 5.2). We assume that, in the initial state, the $3d$ down-spin states are filled and $3d$ holes exist in the up-spin state: we take the positive z-axis as the direction of the magnetization. The $2p$-core electron can be photoexcited into the d or s symmetry state by the dipole transition.

We first consider the $2p \rightarrow d$ transition. As the transition probability from the $2p$ state $|\xi\rangle$ with the azimuthal quantum number m_ξ to the d symmetry state with the quantum number $m = m_\xi + \mu$ is proportional to $|c^1(2\,(m_\xi + \mu), 1\, m_\xi)|^2$

(see eq. (2.29)). The probability-ratio of both the $1 \rightarrow 2$, $0 \rightarrow 1$ and $-1 \rightarrow 0$ transitions by positive helicity X-ray and the $-1 \rightarrow -2$, $0 \rightarrow -1$ and $1 \rightarrow 0$ transitions by negative helicity is $6 : 3 : 1$ (see Fig. 4.2, where now m_ν should be replaced by m). In the final states corresponding to the $2p_{1/2}$ peak of $2p$ XPS, the $2p$ hole is mainly in the $m_\xi = 1$ state with down-spin or in the $m_\xi = -1$ state with up-spin (see Fig. 5.1(a)). If we note the above-mentioned transition-probability-ratio, the former (latter) state is mainly produced by positive (negative) helicity with emitting the down (up) spin photoelectrons and rather contributes to the higher (lower) binding-energy region of the $2p_{1/2}$ peak due to the $2p$-$3d$ exchange part of the intraatomic electrostatic interactions; the $3d$ and $2p$ holes have the opposite (same) spin to each other in the former (latter). In the final states corresponding to the $2p_{3/2}$ peak, on the other hand, the $2p$ hole is mainly in the $m_\xi = 1$ state with up-spin or in the $m_\xi = -1$ state with down-spin. The former (latter) state is mainly produced by the positive (negative) helicity by emitting photoelectrons with up (down) spin and rather contributes to the lower (higher) binding-energy region of the $2p_{3/2}$ peak due to the $2p$-$3d$ exchange interactions(Fig. 5.1(b)). The MCD in $2p$ XPS for the present case is therefore schematically given as in Fig. 5.1(c).

Next we consider the $2p \rightarrow s$ transition. The final state corresponding to the $2p_{1/2}$ peak with a $2p$ hole mainly in the $m_\xi = 1$ with down-spin ($m_\xi = -1$ with up-spin) orbital, which rather contributes to the higher (lower) binding-energy region of the peak, is in this case produced by negative (positive) helicity unlike the case of $2p \rightarrow d$ transition. On the other hand, the final state corresponding to the $2p_{3/2}$ peak with a $2p$ hole mainly in the $m_\xi = 1$ with up-

spin ($m_\xi = -1$ with down-spin) orbital, which rather contributes to the lower (higher) binding-energy region of the $2p_{3/2}$ peak is produced by negative (positive) helicity. The MCD feature of $2p$ XPS for the $2p \rightarrow s$ process therefore becomes that where the roles of positive and negative helicities in the $2p \rightarrow d$ process are interchanged (see Fig. 5.1(d)).

Since the $2p \rightarrow d$ process is usually dominant compared with the $2p \rightarrow s$, the MCD feature expected in the former process (see Fig. 5.1(c)) is supposed to emerge in the Fe $2p$ XPS experiment. In Fig. 5.2 we show atomic calculations of $2p \rightarrow d$ (a) and $2p \rightarrow s$ (b) XPS spin-resolved spectra for both positive and negative helicities and MCD of $2p$ XPS for 'ferromagnetic' $3d^8$. Slater's integrals F's and G's and spin-orbit interaction ζ's are assumed as follows: $F_d^2 = 9.79$, $F_d^4 = 6.08$ and $\zeta_d = 0$ for the initial state, and $F_d^2 = 11.2$, $F_d^4 = 7.01$, $F_{pd}^2 = 6.68$, $G_{pd}^1 = 5.07$, $G_{pd}^3 = 2.88$, $\zeta_d = 0.112$ and $\zeta_p = 11.51$ for the final state, all in units of eV. The crystalline field $10Dq = 1.0$eV and the molecular field $\mu_B \mathcal{H} = 0.02$eV on spin (see eq. (4.2)) are adopted. We see that the spin-resolved XPS expected from the above-mentioned discussion and an essential feature of MCD schematically shown in Fig. 5.1 are realized. Our calculation seems to give a kind of justification for an analysis of MCD data with use of the phenomenological valence-core exchange. It is also worth mentioning that the MCD spectrum for $2p \rightarrow s$ is obtained exactly by interchanging the role of positive and negative helicities in that for $2p \rightarrow d$, which can be easily shown by using properties of the c^1's. We note that the essence of our discussion also applies to the $3d$-core XPS in rare-earths with a spin-dominant magnetic moment, such as Gd^{3+} with the ground state ^8S under an infinitesimal magnetic

field, if we replace the discussions for $2p_{1/2}$ and $2p_{3/2}$ peaks in $2p \rightarrow d$ (s) transition by those for $3d_{3/2}$ and $3d_{5/2}$ peaks in $3d \rightarrow f$ (p), respectively.

§3. Orbital-moment-dominant Magnetic state

Next we go into a discussion on the case where the orbital moment mainly contributes to the atomic magnetic moment. Such cases are often seen in rare-earth ferromagnets. In order to demonstrate that the MCD feature different from that for spin-dominant system is realized, we consider, as an example, the $3d$ XPS in Ce^{3+} $(4f^1)$ with the ground state $^2F_{5/2}$ under an infinitesimal magnetic field: the $4f$ state $|\nu\rangle$ with the azimuthal quantum number $m_\nu = -3$ and up-spin is dominantly occupied.

We consider the $3d \rightarrow f$ transition. The transition-probability from the $3d$ state $|\xi\rangle$ with the azimuthal quantum number m_ξ to f symmetry state with the quantum number $m = m_\xi + \mu$ is proportional to $|c^1(3\,(m_\xi + \mu), 2\,m_\xi)|^2$. The probability-ratio of both the $2 \rightarrow 3$, $1 \rightarrow 2$, $0 \rightarrow 1$, $-1 \rightarrow 0$ and $-2 \rightarrow -1$ transitions by positive helicity and the $-2 \rightarrow -3$, $-1 \rightarrow -2$, $0 \rightarrow -1$, $1 \rightarrow 0$ and $2 \rightarrow 1$ transitions by negative helicity is $15 : 10 : 6 : 3 : 1$ (see Fig. 3.4). In the final state, the exchange interaction between a pre-existing $4f$ electron and a photo-produced $3d$ hole, if they have the same spin, lifts up the final-state-energy by an amount mainly determined by the Slater integral G^1 multiplied by $|c^1(3\,m_\nu, 2\,m_\xi)|^2$. The final state corresponding to the $3d_{3/2}$ peak of $3d$ XPS has a $3d$ hole mainly in the orbital with either positive m_ξ and down-spin or negative m_ξ and up-spin. The former (latter) is seen to be dominantly produced by the positive (negative) helicity and rather contributes to the lower (higher)

binding-energy region of the peak due to the $3d$-$4f$ exchange interaction. The final state corresponding to the $3d_{5/2}$ peak, on the other hand, has a $3d$ hole mainly in the orbital with either positive m_ξ and up-spin or negative m_ξ and down-spin. The former (latter) state with up-spin (down-spin) hole is seen to be dominantly produced by the positive (negative) helicity. The magnitude of the $3d$-$4f$ exchange interaction between the pre-existing $4f$ electron mainly in the $m_\nu = -3$ and up-spin state and the core-hole is, however, small compared with the $3d_{3/2}$ case for both final states produced by positive and negative helicities, because the G^1-exchange interaction is suppressed by the above-mentioned prefactor in the former case and by a 'spin-mismatch' in the latter case; both final states do not 'prefer' either the higher or the lower binding-energy region of the $3d_{5/2}$ peak. The feature of MCD in the $3d_{5/2}$ region is therefore expected not to be so simple and will be, if the lifetime-broadening of spectrum is taken into account, less prominent compared with the $3d_{3/2}$ case.

In Fig. 5.3, we show the calculated spin-resolved $3d \rightarrow f$ (a) and $3d \rightarrow p$ (b) XPS and MCD in the present case with use of the Slater integrals and spin-orbit interactions given by Thole *et al.*[54] In the $3d_{3/2}$ region for $3d \rightarrow f$, a clear MCD is in fact seen, which is opposite to that in $2p_{1/2}$ region for $2p \rightarrow d$ shown in Fig. 5.3 reflecting the spin-moment being antiparallel to the magnetization-direction. In the $3d_{5/2}$ region, on the other hand, the MCD pattern is seen to be not so simple. For $3d \rightarrow p$ transition, we again have MCD obtained by replacing positive and negative helicities in $3d \rightarrow f$.

§4. Conclusion

We have given basic features of MCD in $2p$ XPS and $3d$ XPS for the two types of ferromagnet where mainly the spin and orbital moment respectively contribute to the magnetic moment, with use of an atomic model including multiplet effect, and without use of a phenomenological core-valence exchange model. The MCD feature, which depends on whether spin or orbital moment mainly contributes to magnetic moment, is expected to be a powerful characteristic to probe the atomic magnetic state in ferromagnets. We furthermore showed that the usefulness of the characteristic is increased by carrying out spin-resolved photoemission. Our calculation preassume the dipole-transition probability being independent of the photoelectron energy ω. This is justified for the experimental condition[39] with $\omega \sim 100$eV. We have concentrated our discussion not on the absolute values but on patterns of MCD, the former of which will need considerations about various origins to reduce MCD. *

* The content of this chapter was presented on March 25 in 1991.[49] After preparing publication,[48] we found a paper by van der Laan discussing a similar subject.[52]

Charpter VI

Summary

We calculated the magnetic dichroism in $3d \rightarrow 4f$ and $4d \rightarrow 4f$ XAS and $3d$ XPS of rare earth ions under an infinitesimal molecular field on the total angular momentum, and that in $2p \rightarrow 3d$ XAS and $2p$ XPS of transition element ions under a crystalline field and a molecular field on the spin.

Through the calculations, magnetic dichroism in core XAS and core XPS was found to reflect the spin and orbital moment states of the magnetic orbit very well, in such ways that XAS and XPS, and spectroscopies exciting different core orbits, give complementary information. The effect of rather weak field as the uniaxial field that works on Co^{2+} in $CoFe_2O_4$ was found to be considerably large. We also succeeded in interpreting the observed MCD in $2p$ XAS of Co in $CoFe_2O_4$, that in $3d$ and $4d$ XAS of Gd, and in $2p$ XPS of iron.

The relation between the main features in the magnetic dichroism and the character of the symmetry breaking in the spin and orbital-moment state of the initial state was explained in a common scheme. The important factors were found to be the transition operators of the photoexcitation by the polarized photon, the spin-orbit interaction of the photoproduced core hole, and the electrostatic interaction between the core hole and the valence electrons.

Through our calculations and discussions, we have shown the capability of the magnetic dichroism in the soft X-ray region as a good tool in investigating the magnetic states. The characteristics of the information that can be

yielded were shown to be as follows: it can be directly connected with the spin and orbital-moment state; information from various aspects are provided by changing the core whose electron is photoexcited and by measuring photoemission and phtoabsorption; multiplet structures in the spectra is sensitive to the detailed magnetic state.

Acknowledgments

I would like to express my sincere thanks to Professor Takeo Jo. He has introduced me to this interesting topic, and fruitful discussions with him and his advices have been quite a help throughout the period of this study.

I would also like to thank Professor Junjiro Kanamori for critical and helpful discussions. Particularly, his suggestion about the uniaxial potential on the cobalt ion in cobalt ferrite led the discussion to a new stage.

Drs. F. Sette and C. T. Chen, and Professor Tsuneaki Miyahara deserve special acknowledgments for providing their experimental data prior to publication.

At last, but not the least, I would like to thank the colleagues at Kanamori Lab. for discussions and practical helps.

References

1) Physica Scripta **T31** (1990), Proceedings of The 9th International Conference on Vacuum Ultraviolet Radiation Physics.

2) L. C. Davis, J. Appl. Phys. **59**, R25 (1986).

3) K. A. Gschneidner, L.-R. Eyring and S. Hüfner (eds.), *Handbook on the Physics and Chemistry of Rare Earths* vol. 10 (Elsevier Science Publishers B.V., North-Holland 1987).

4) M. Cardona and L. Ley (eds.), *Photoemission in Solids* I, II (Springer-Verlag, Berlin, 1978, 1979).

5) E.-E. Koch (ed.), *Handbook on Synchrotron Radiation* Vol. 1A, 1B (North-Holland Publishing Company, Amsterdam, 1983).

6) J. Kanamori and A. Kotani (eds.), *Core-Level Spectroscopy in Condensed Systems*, (Springer-Verlag, Berlin, 1987).

7) C. Kunz (ed.), *Synchrotron Radiation*, (Springer-Verlag, Berlin, 1979).

8) G. A. Sawatzky, p 99 in ref. 6

9) A. Kotani, T. Jo and J. C. Parlebas, Adv. Phys. **37**, 37 (1988).

10) T. Jo, J. Phys. Soc. Jpn. **58**, 1452 (1989).

11) S. Imada and T. Jo, J. Phys. Soc. Jpn. **58**, 402 (1989).

12) S. Imada and T. Jo, J. Phys. Soc. Jpn. **58**, 2665 (1989).

13) S. Imada and T. Jo, Physica Scripta **41**, 115 (1990).

14) C. T. Chen, F. Sette, Y. Ma and S. Modesti, Phys. Rev. B**42**, 7262 (1990).

15) T. Koide, T. Shidara, H. Fukutani, K. Yamaguchi, A. Fujimori and S. Kimura, to be published in Phys. Rev. B.

16) S. Yamamoto, H. Kawata, H. Kitamura M. Ando, N. Saki and N. Shiotani, Phys Rev. Lett. **62**, 2672 (1989).

17) E. U. Condon and G. H. Shortley, *The Theory of Atomic Spectra*, (Cambridge University Press, London, 1964).

18) B. T. Thole, G. van der Laan and G. A. Sawatzky, Phys. Rev. Lett. **55**, 2086 (1985).

19) G. van der Laan, B. T. Thole, G. A. Sawatzky, J. B. Goedkoop, J. C. Fuggle, J.-M. Esteva, R. Karnatak, J. P. Remeika and H. A. Dabkowska, Phys. Rev. B**34**, 6529 (1986).

20) J. B. Goedkoop, B. T. Thole, G. van der Laan, G. A. Sawatzky, F. M. F. de Groot and J. C. Fuggle, Phys. Rev. B**37**, 2086 (1988).

21) J. B. Goedkoop, M. Grioni and J. C. Fuggle, Phys. Rev. B**43**, 1179 (1991).

22) R. J. H. Kappert, M. Sacchi, J. B. Goedkoop, M. Grioni and J. C. Fuggle, submitted to Surf. Science Lett.

23) M. Sacchi, O. Sakho and G. Rossi, Phys. Rev. B**43**, 1276 (1991).

24) G. Schütz, W. Wagner, W. Wilhelm, P. Kienle, R. Zeller, R. Frahm and G. Materlik, Phys. Rev. Lett. **58**, 737 (1987).

25) F. Baudelet, E. D. Dartyge, G. Krill, J. P. Kappler, C. Brouder, M. Piecuch and A. Fontaine, submitted to Phys. Rev.

26) H. Maruyama, T. Iwazumi, H. Kawata, A. Koizumi, M. Fujita, H. Sakurai, F. Itoh, K. Namikawa, H. Yamasaki and M. Ando, J. Phys. Soc. Jpn. **60**, No. 5 (1991).

27) S. P. Collins, M. J. Cooper, A. Brahmia, D. Laundy and T. Pitkanen, J. Phys. Condens. Matter **1**, 326 (1989).

28) H. Ebert, B. Drittler, R. Zeller and G. Schütz, Solid State Commun. **69**, 485 (1989).

29) G. Schütz, M. Knülle, R. Wienke, W. Wilhelm, W. Wagner, P. Kienle and R. Frahm, Z. Phys. B, Condens. Matter **73**, 67 (1988).

30) P. Fischer, G. Schütz and G. Wiesinger, Solid State Commun. **76**, 777 (1990).

31) H. Ebert, P. Strange and B. L. Gyorffy, J. Appl. Phys. **63**, 3055 (1988); J. Phys. (Paris) Colloq. 49, C8-31 (1988).

32) P. Strange, H. Ebert, J. B. Staunton and B. L. Gyorffy, J. Phys. Condens. Matter **1**, 2959 (1989).

33) H. Ebert and R. Zeller, Physica B+C **161B**, 191 (1989); Phys. Rev. B**42**, 2774 (1990).

34) P. Carra and M. Altarelli, Phys. Rev. Lett. **64**, 1286 (1990).

35) P. Carra B. N. Harmon, B. T. Thole, M. Altarelli and G. A. Sawatzky, Phys. Rev. Lett. **66**, 2495 (1991).

36) F. Sette, C. T. Chen, Y. Ma, S. Modesti and N. V. Smith, AIP Conference Proceedings **215**, 787 (1990).

37) S. Muto *et al.*, Anual Meetings of Japanese Society for Synchrotron Radiation Research(1991), O4-5; T. Miyahara *et al.*, private communication.

38) T. Miyahara *et al.*, private communication.

39) L. Baumgarten, C. M. Schneider, H. Petersen, F. Schäfers and J. Kirschner, Phys. Rev. Lett. **65**, 492 (1990).

40) T. Jo and S. Imada, J. Phys. Soc. Jpn. **58**, 1922 (1989).

41) T. Jo and S. Imada, J. Phys. Soc. Jpn. **59**, 1421 (1990).

42) T. Jo and S. Imada, Physica Scripta. **41**, 560 (1990).

43) S. Imada and T. Jo, J. Phys. Soc. Jpn. **59**, 3358 (1990).

44) J. L. Erskine and E. A. Stern, Phys. Rev. B**12**, 5016 (1975).

45) J. B. Goedkoop, J. C. Fuggle, B. T. Thole, G. van der Laan and G. A. Sawatzky, Nucl. Instrum. Methods A**273**, 429 (1988).

46) S. Imada and T. Jo, Sectional Meetings of the Physical Society of Japan, October 2, 1991, 2pW12.

47) S. Imada and T. Jo, submitted to J. Magn. Magn. Mater. (Proc. of Intl. Conf. Magnetism).

48) S. Imada and T. Jo, J. Phys. Soc. Jpn. **60**, No. 9 (1991).

49) T. Jo and S. Imada, Sectional Meetings of the Physical Society of Japan, March 25, 1991, 25pW17.

50) T. Jo and G. A. Sawatzky, Phys. Rev. B**43**, 8771 (1991).

51) C. T. Chen, N. V. Smith and F. Sette, Phys. Rev. B**43**, 6785 (1991).

52) G. van der Laan, Phys. Rev. Lett. **66**, 2527 (1991).

53) G. van der Laan and B. T. Thole, Phys. Rev. B**43**, 13401 (1990).

54) B. T. Thole, G. van der Laan, J. C. Fuggle, G. A. Sawatzky, R. C. Karnatak and J.-M. Esteva, Phys. Rev. B**32**, 5107 (1985).

55) J. Sugar, Phys. Rev. B**5**, 1785 (1972).

56) J. C. Slonczewski, Phys. Rev. **110**, 1341 (1958).

57) M. Tachiki, Prog. Theor. Phys. **23** 1055 (1960).

58) F. M. F. de Groot, J. C. Fuggle, B. T. Thole and S. A. Sawatzky, Phys.

Rev. B**42**, 5459 (1990).

59) J. Smit and H. P. J. Wijn, *Ferrites*, (N. V. Philips' Gloeilampenfabrieken, Eindhoven, the Netherlands, 1959).

Table I. Parameters of Slater's integral and spin-orbit interaction used in the calculation of $3d$ and $4d$ XAS of rare earth ions[54,55] (all values in eV; see eqs. (2.2) and (2.9)).

N	Ce^{3+} 1	Pr^{3+} 2	Nd^{3+} 3	Pm^{3+} 4	Sm^{3+} 5	Eu^{3+} 6	Gd^{3+} 7	Tb^{3+} 8	Dy^{3+} 9	Ho^{3+} 10	Er^{3+} 11	Tm^{3+} 12
$3d^{10}4f^N$												
$F^2_{(f)}$		9.78	10.18	10.56	10.92	11.27	11.60	11.93	12.25	12.57	12.87	13.18
$F^4_{(f)}$		6.14	6.39	6.63	6.85	7.07	7.28	7.49	7.69	7.88	8.08	8.26
$F^6_{(f)}$		4.41	4.60	4.77	4.93	5.09	5.24	5.39	5.53	5.67	5.81	5.94
ζ_f	0.087	0.103	0.114	0.136	0.155	0.175	0.197	0.221	0.246	0.273	0.302	0.333
$3d^9 4f^{N+1}$												
$F^2_{(f)}$	10.10	10.48	10.84	11.18	11.51	11.84	12.16	12.47	12.77	13.07	13.37	
$F^4_{(f)}$	6.35	6.59	6.81	7.03	7.24	7.44	7.64	7.84	8.03	8.21	8.40	
$F^6_{(f)}$	4.57	4.74	4.91	5.07	5.21	5.36	5.50	5.64	5.78	5.91	6.04	
$F^2_{(fd)}$	5.99	6.31	6.62	6.92	7.21	7.50	7.77	8.04	8.31	8.57	8.83	9.09
$F^4_{(fd)}$	2.71	2.87	3.03	3.19	3.34	3.49	3.63	3.77	3.91	4.04	4.18	4.31
$G^1_{(fd)}$	4.06	4.33	4.59	4.84	5.09	5.33	5.56	5.79	6.02	6.24	6.46	6.68
$G^3_{(fd)}$	2.37	2.53	2.69	2.83	2.98	3.12	3.26	3.40	3.53	3.66	3.79	3.92
$G^5_{(fd)}$	1.64	1.75	1.85	1.96	2.06	2.16	2.25	3.35	2.44	2.53	2.62	2.71
ζ_d	7.45	8.14	8.88	9.67	10.51	11.41	12.36	13.37	14.44	15.57	16.78	18.05
ζ_f	0.107	0.124	0.135	0.160	0.180	0.202	0.226	0.251	0.278	0.307	0.338	0.371
$4d^9 4f^{N+1}$												
$F^2_{(f)}$	9.13	9.69	10.2	10.7	11.0	11.2	11.3	11.6	11.9	12.35	12.81	
$F^4_{(f)}$	6.59	7.27	7.8	8.1	8.3	8.4	8.5	8.6	8.8	9.25	10.07	
$F^6_{(f)}$	4.80	4.16	4.9	5.2	5.5	5.8	6.1	6.3	6.6	6.92	7.14	
$F^2_{(fd)}$	10.3	10.7	11.2	11.8	12.3	12.5	12.5	12.6	12.8	13.2	13.8	14.2
$F^4_{(fd)}$	6.6	6.8	7.1	7.5	7.8	8.0	8.0	8.0	8.2	8.4	8.8	9.1
$G^1_{(fd)}$	10.13	11.3	11.8	12.2	12.4	12.5	12.4	12.6	13.1	14.1	14.7	14.6
$G^3_{(fd)}$	6.36	7.12	7.5	7.7	7.8	7.85	7.81	8.0	8.3	8.88	9.26	9.20
$G^5_{(fd)}$	4.49	5.03	5.3	5.4	5.5	5.57	5.52	5.6	5.9	6.27	6.54	6.50
ζ_d	1.35	1.52	1.7	1.9	2.1	2.22	2.42	2.7	2.9	3.05	3.28	3.52
ζ_f	0.092	0.113	0.13	0.15	0.17	0.174	0.236	0.24	0.27	0.295	0.327	0.361

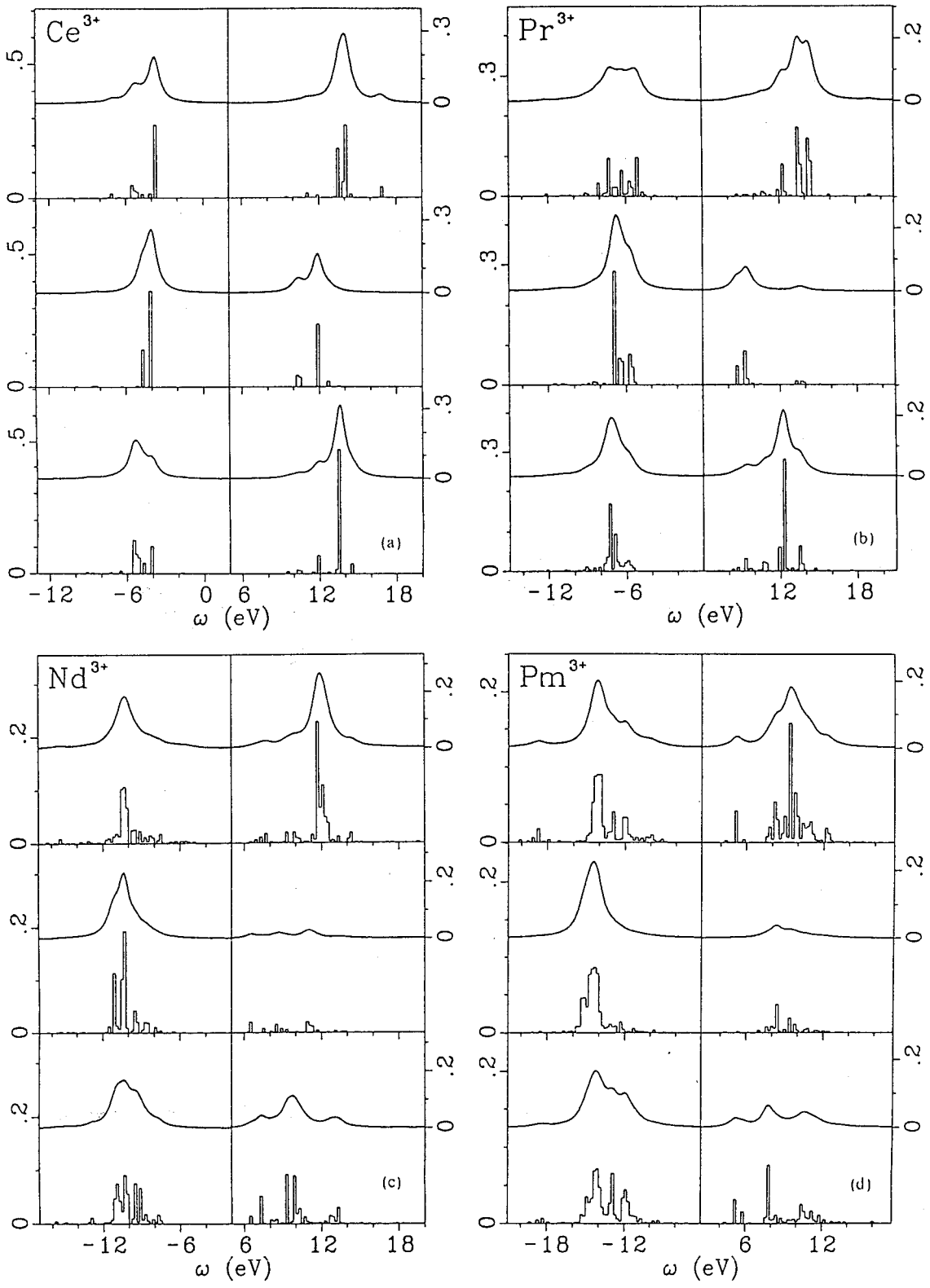

Fig. 3.1. The calculated $3d$ XAS of rare earth ions in an infinitesimal molecular field on the total angular momentum, by positive helicity (top), negative helicity (middle), and linear polarization with $\boldsymbol{E} \parallel z$-axis (bottom). $3d_{5/2}$ peak is shown at the left and $3d_{3/2}$ at the right. In each section, the histogram of the absorption lines is shown at the bottom, and the curve of the Lorentzian convolution with $2\Gamma = 1.0$eV at the top. Normalization is taken by the average of the integrated intensities for the three polarizations. The scale for the histogram is shown at the left and that for the convoluted curve at the right. Zero-point of the photon-energy is taken arbitrary.

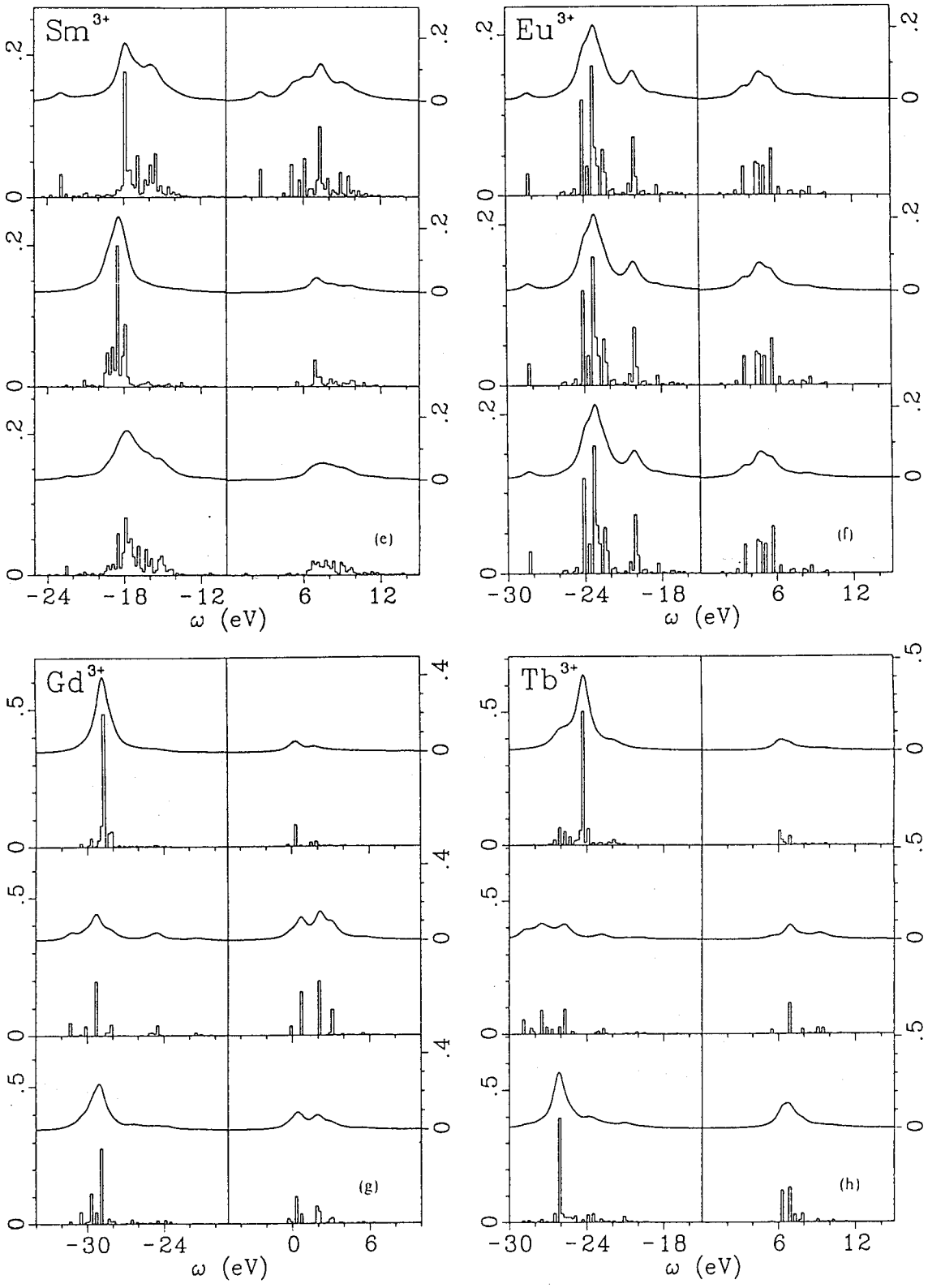

Fig. 3.1 (continued)

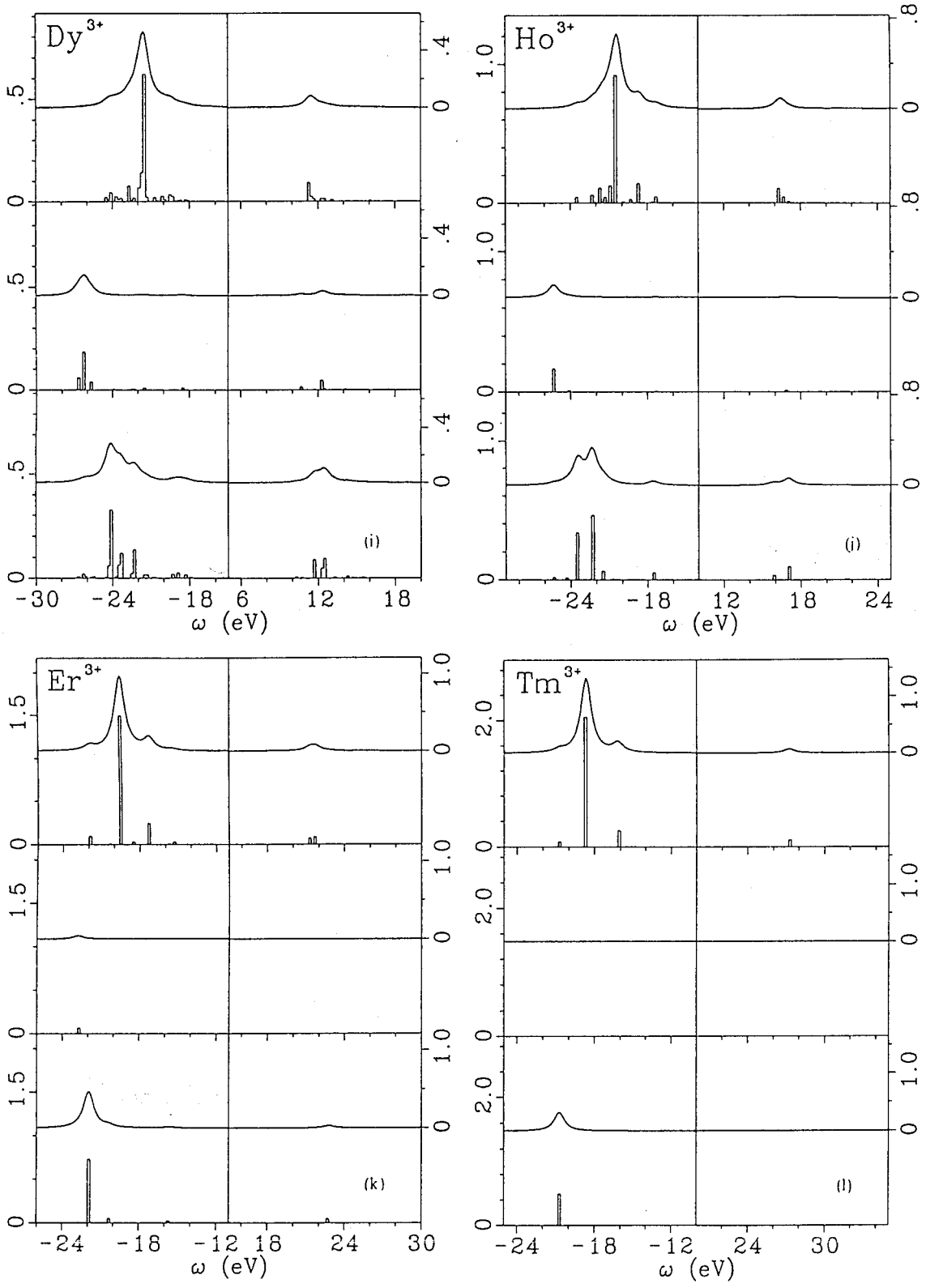

Fig. 3.1 (continued)

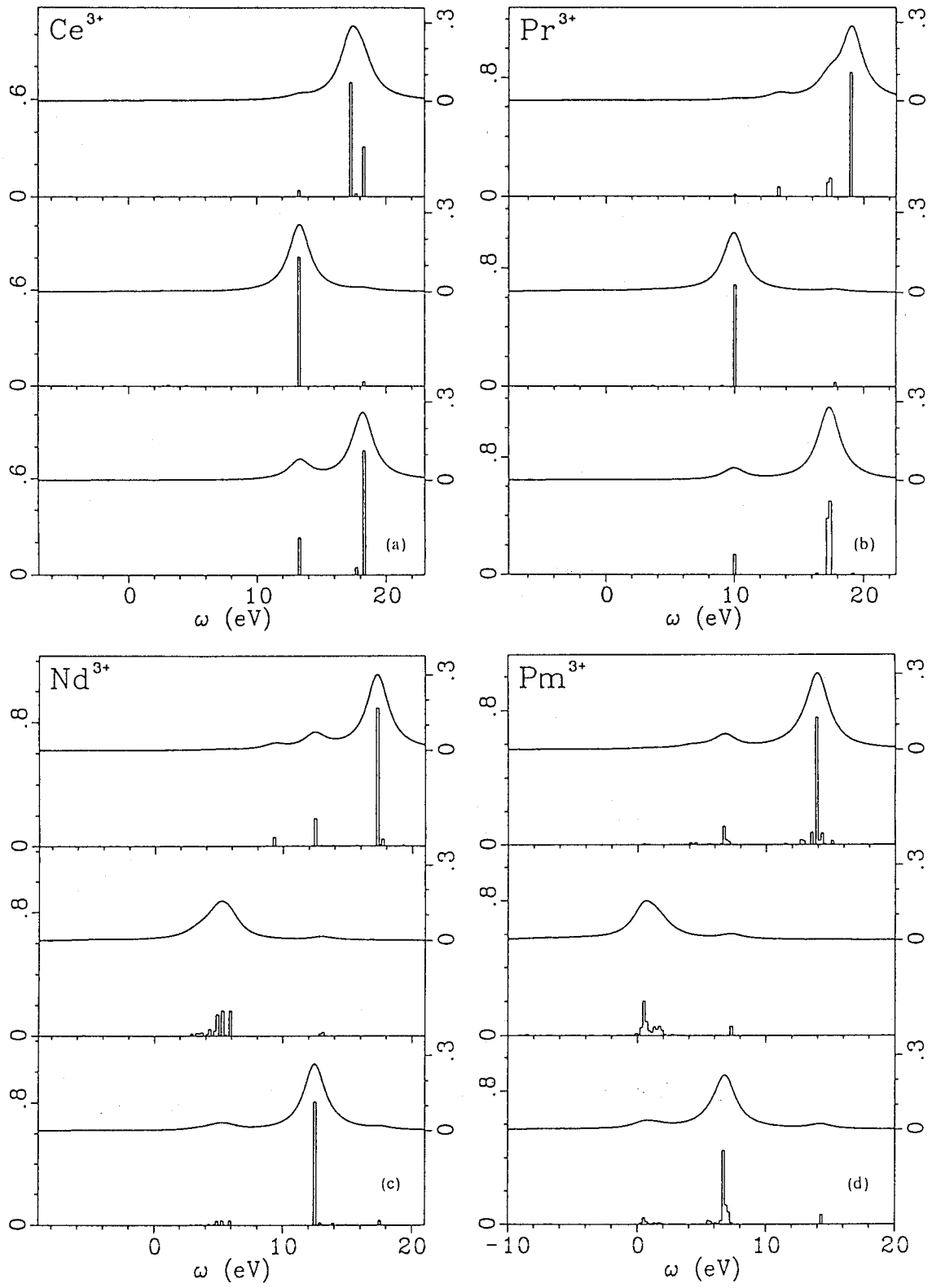

Fig. 3.2. The calculated $4d$ XAS of rare earth ions in an infinitesimal molecular field on the total angular momentum, by positive helicity (top), negative helicity (middle), and linear polarization with $\boldsymbol{E} \parallel z$-axis (bottom). In each section, the histogram of the absorption lines is shown at the bottom, and the curve of the Lorentzian convolution with $2\Gamma = 2.0$eV at the top. The conditions for normalization and scale are the same as Fig. 3.1. Zero-point of the photon-energy is taken arbitrary.

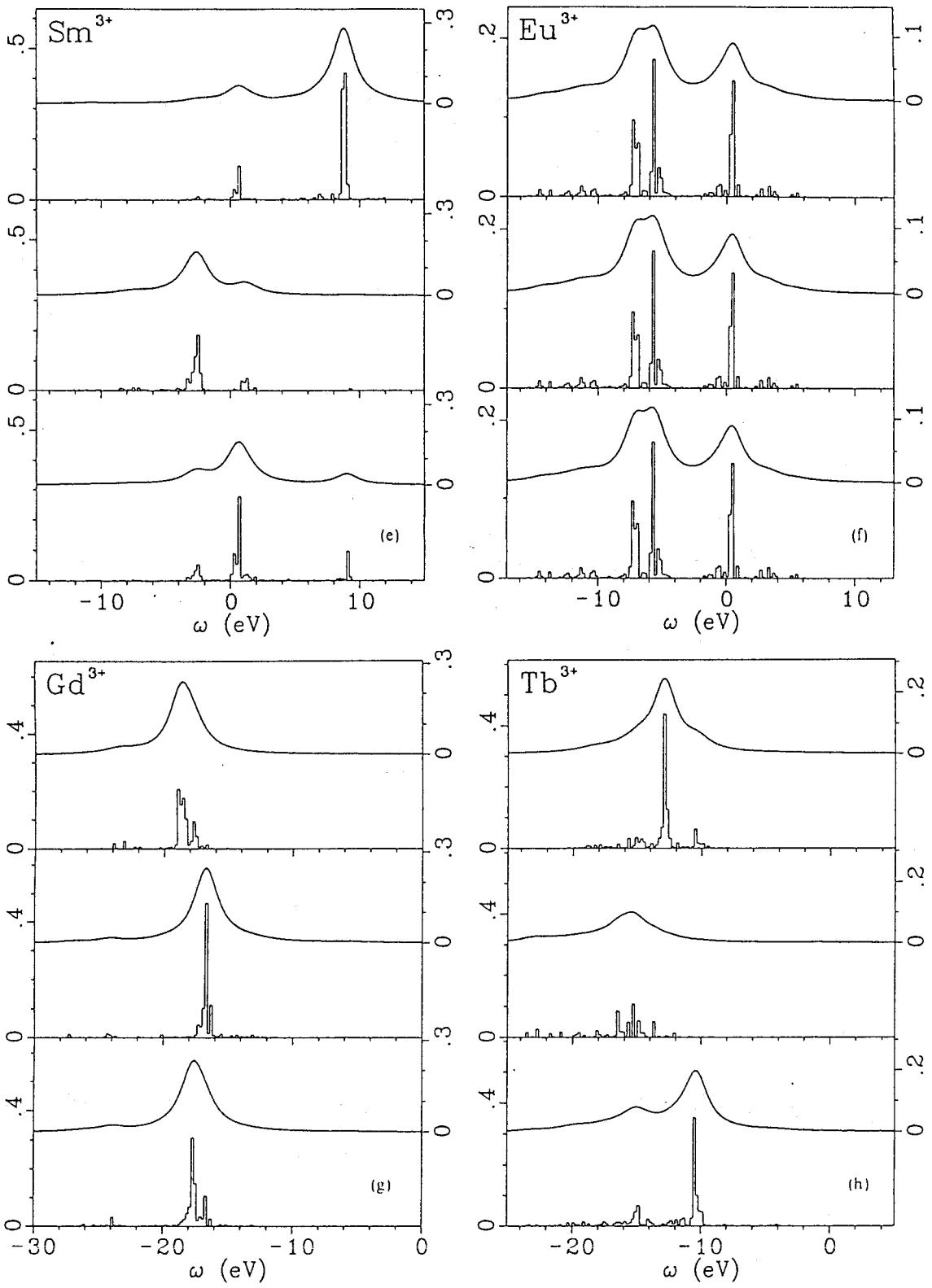

Fig. 3.2 (continued)

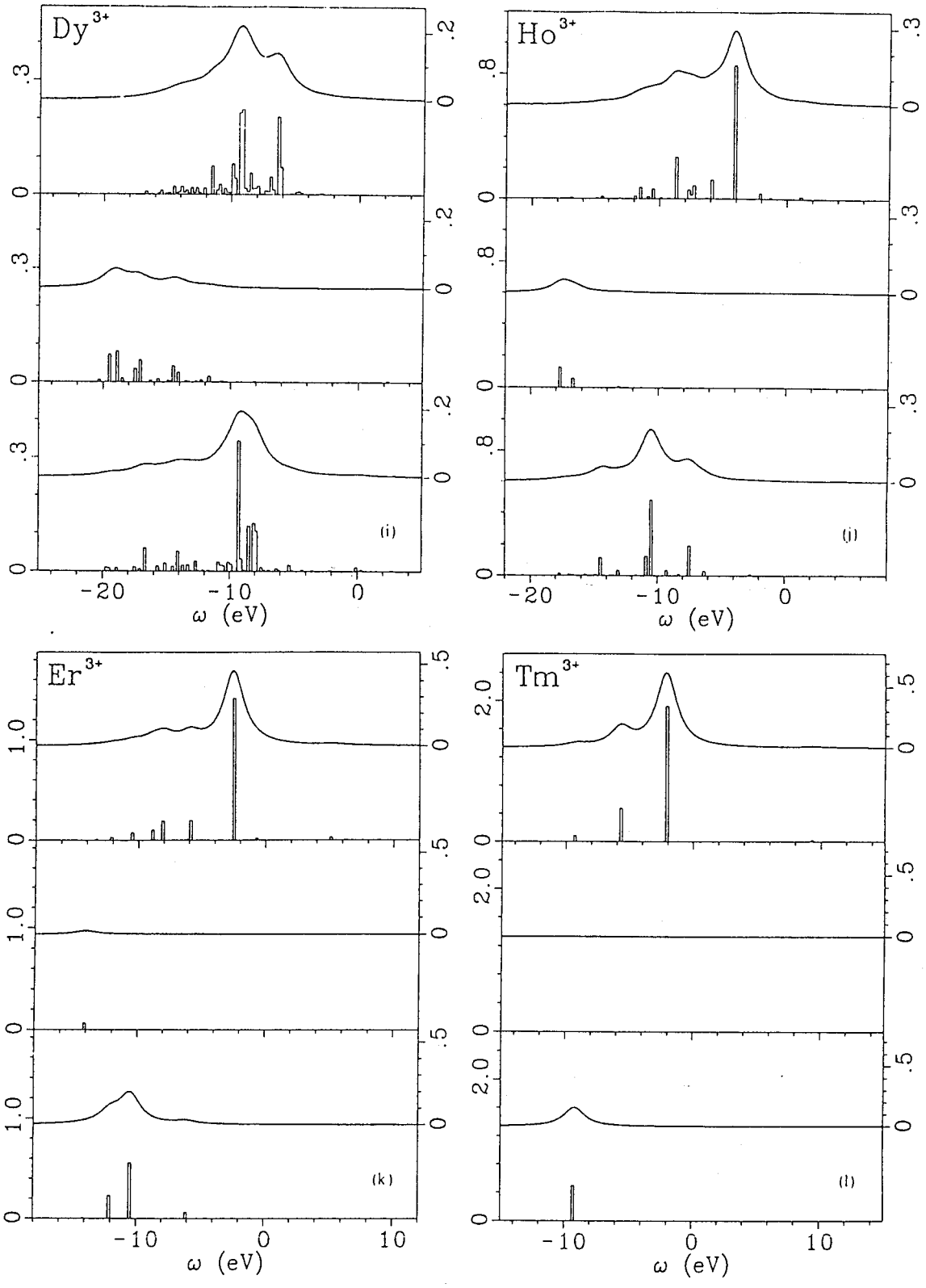

Fig. 3.2 (continued)

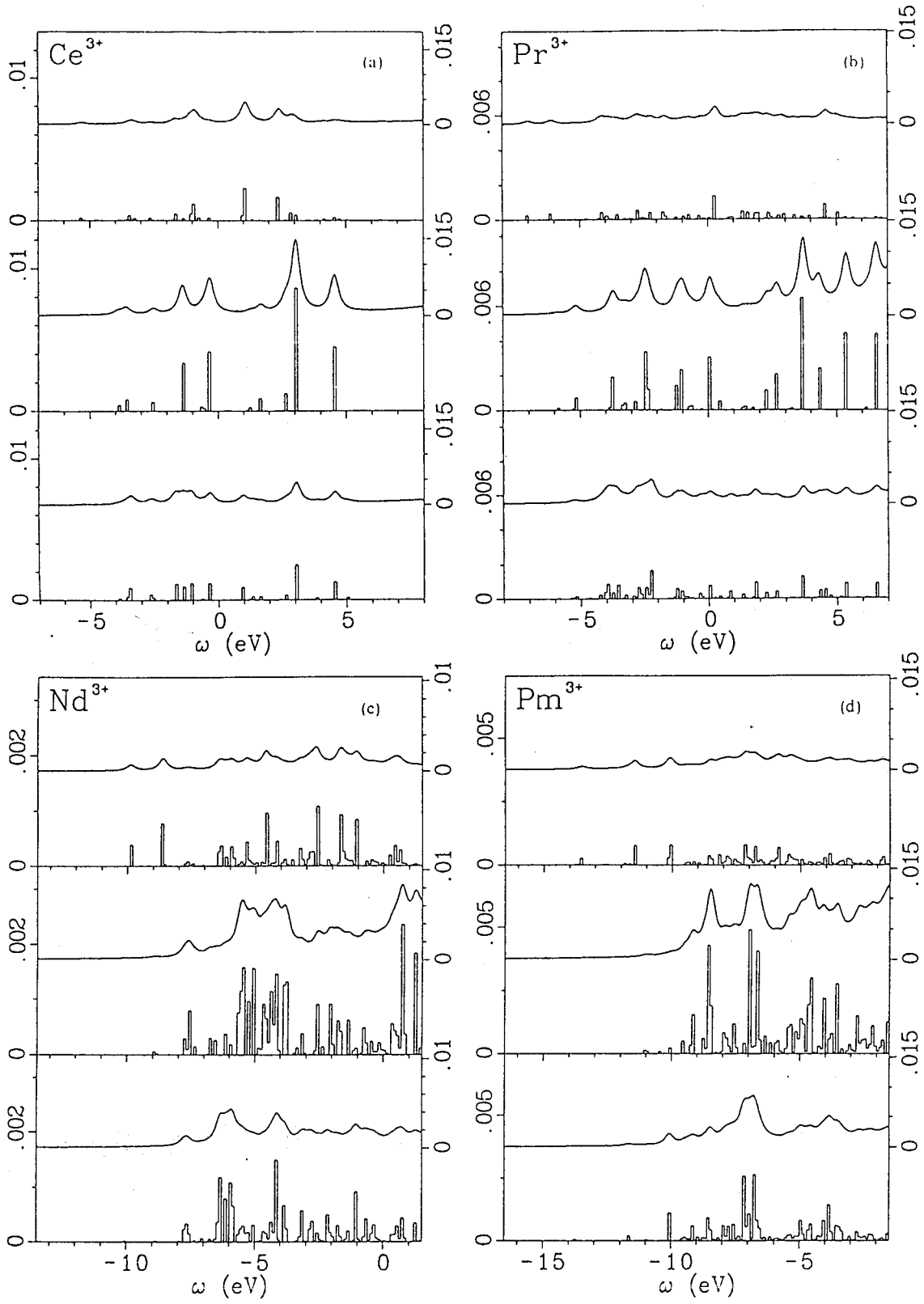

Fig. 3.3. The calculated prethreshold region of $4d$ XAS of rare earth ions in an infinitesimal molecular field on the total angular momentum, by positive helicity (top), negative helicity (middle), and linear polarization with $\boldsymbol{E} \parallel z$-axis (bottom). In each section, the histogram of the absorption lines is shown at the bottom, and the curve of the Lorentzian convolution with $2\Gamma = 0.2$eV at the top. Normalization is taken as in Fig. 3.1 with integration over the whole energy range including the giant resonance peaks. The condition for the scale is the same as Fig. 3.1. Zero-point of the photon-energy is taken the same as in Fig. 3.2.

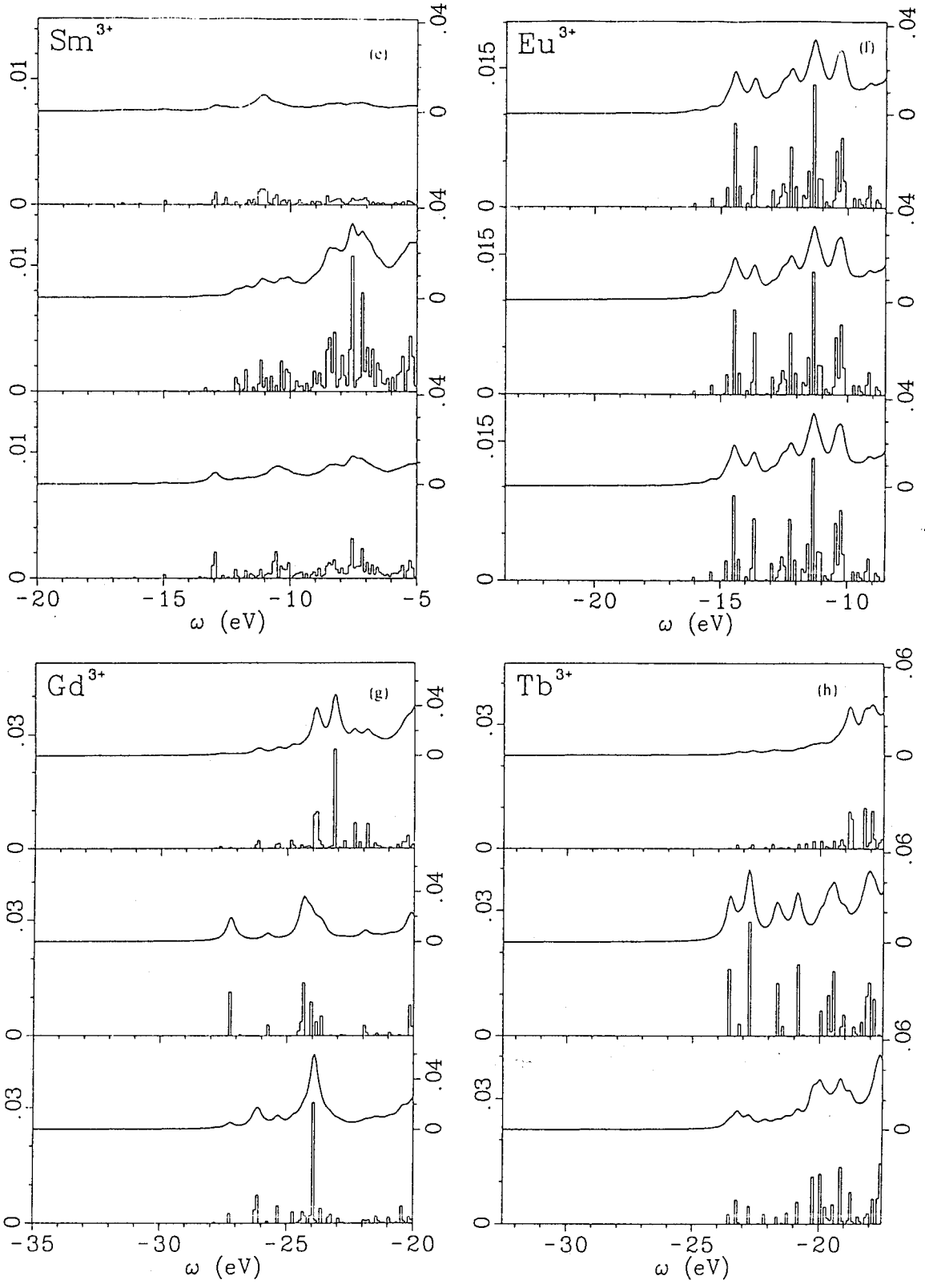

Fig. 3.3 (continued)

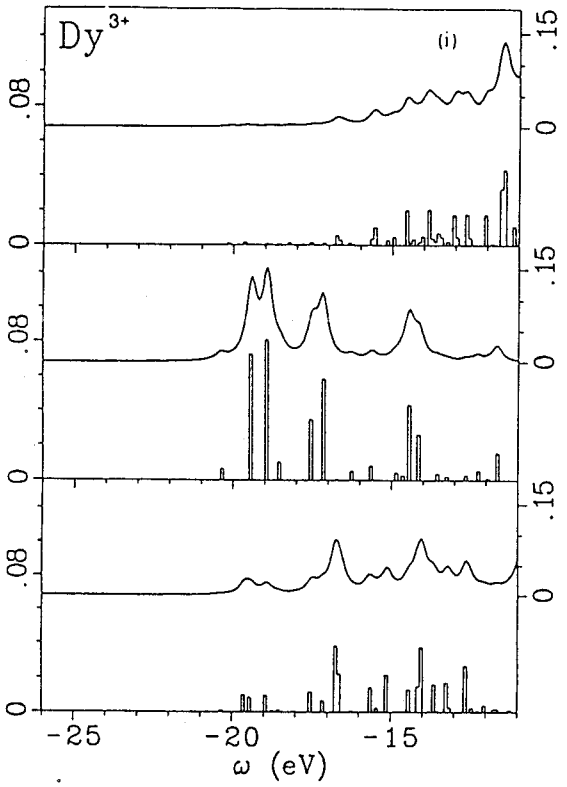

Fig. 3.3 (continued)

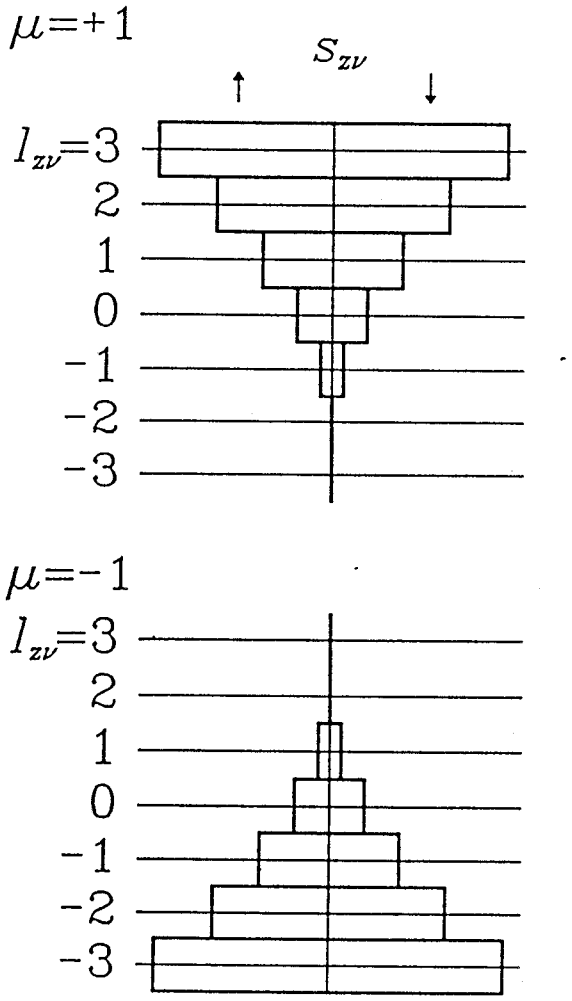

Fig. 3.4. The distribution of $|c^1(3m_\nu, 2\,m_\nu - \mu)|^2$, the weights of the transition to the f states $|\nu\rangle$ in $d \rightarrow f$ photoabsorption by positive helicity($\mu = +1$) and negative helicity($\mu = -1$).

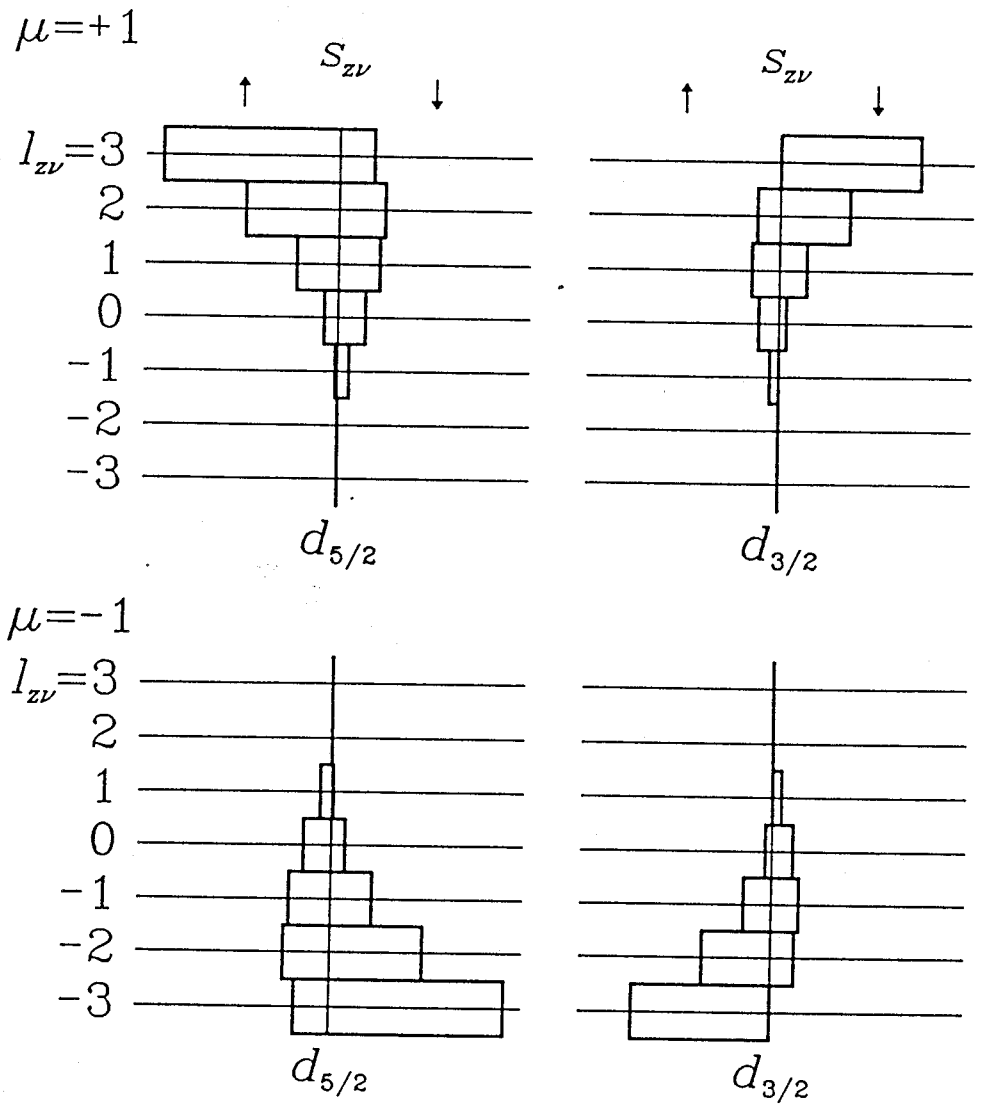

Fig. 3.5. The distribution of the weights of the transition to the f states $|\nu\rangle$ in $d \rightarrow f$ photoabsorption by the light with the polarization μ, when the spin-orbit interaction of the core d hole is strong enough for j of the core hole to be a nearly good quantum number.

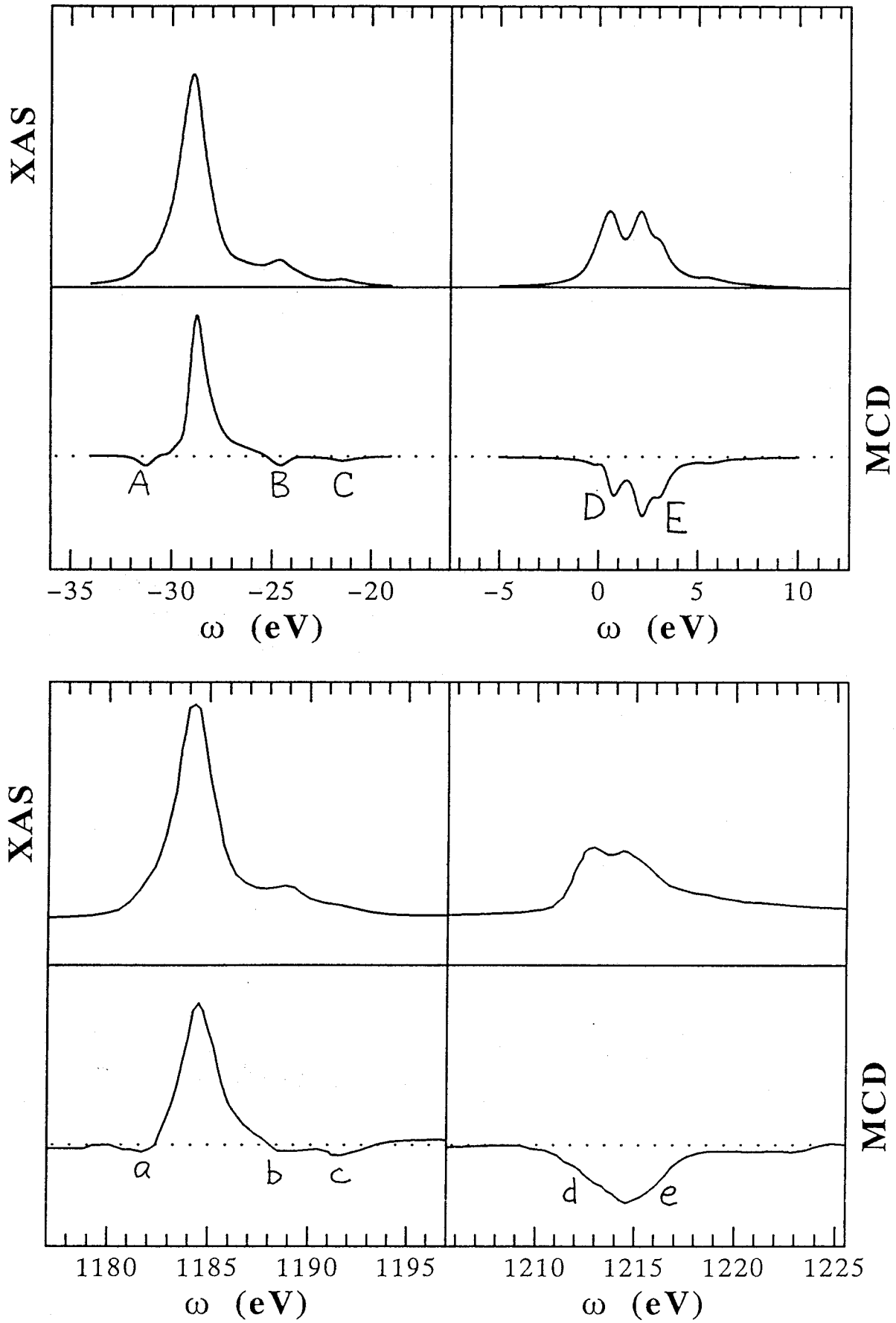

Fig. 3.6. $3d$ XAS of Gd. Top: Calculated spectrum for X-rays without polarization $(I_+ + I_- + I_{\|})/3$ (upper row), and MCD $(I_+ - I_-)/2$ (lower row). Zero-point of the photon-energy is taken arbitrary. Bottom: Observed total spectrum ('I_+'+'I_-')/2 (upper row) and difference spectrum ('I_+'−'I_-')/2 × 14 (lower row) by circularly polarized light of Gd in GdIG.[36] $3d_{5/2}$ peaks are shown at the left and $3d_{3/2}$ at the right.

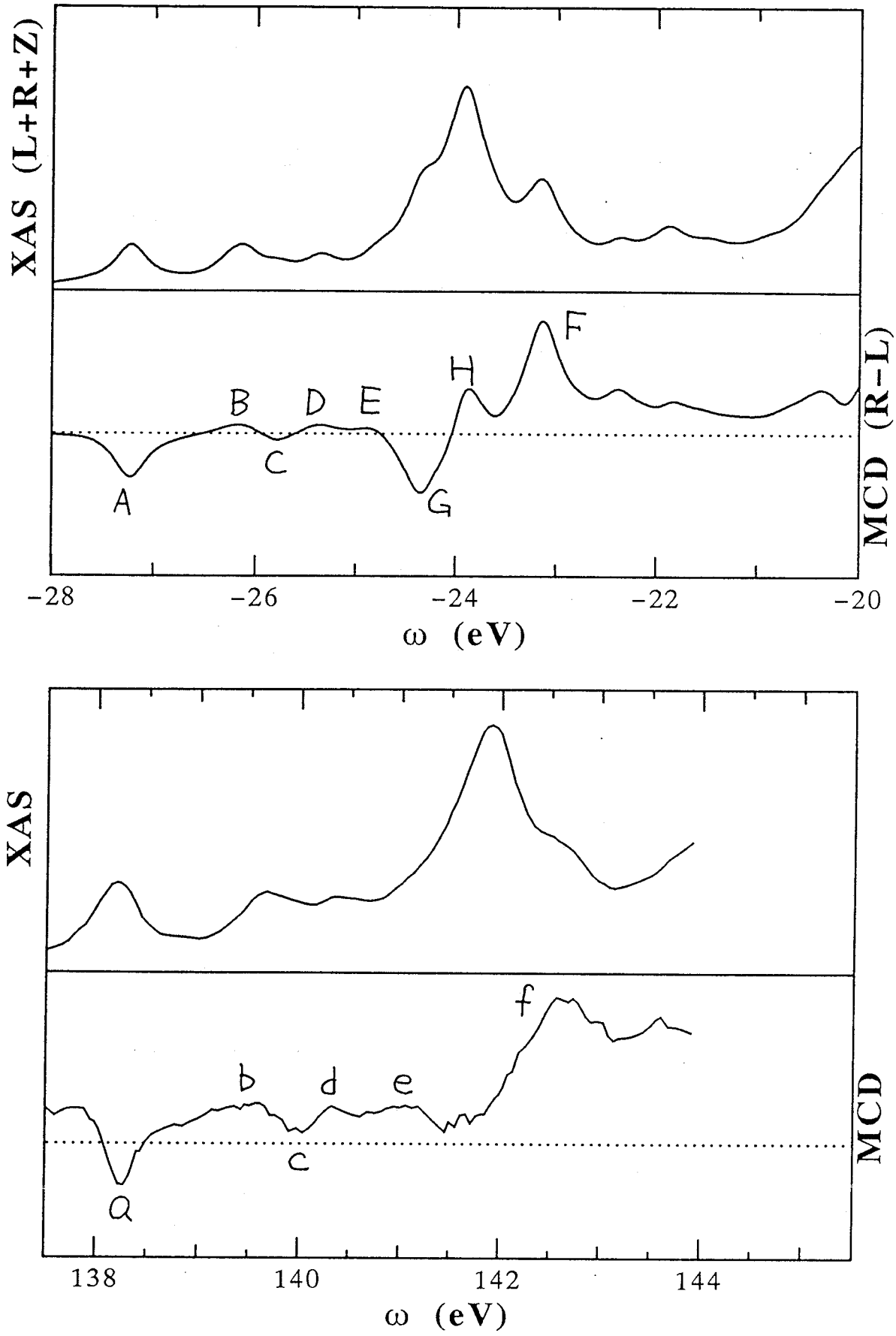

Fig. 3.7. The prethreshold region of $4d$ XAS of Gd. Top: Calculated spectrum for X-rays without polarization $(I_+ + I_- + I_\parallel)/3$ (upper row), and MCD $(I_+ - I_-)/2$ (lower row). Zero-point of the photon-energy is taken arbitrary. Bottom: Observed total spectrum ('I_+'+'I_-')/2 (upper row) and difference spectrum ('I_+'−'I_-')/2 × 4 (lower row) by circularly polarized light of ferromagnetic Gd.[38]

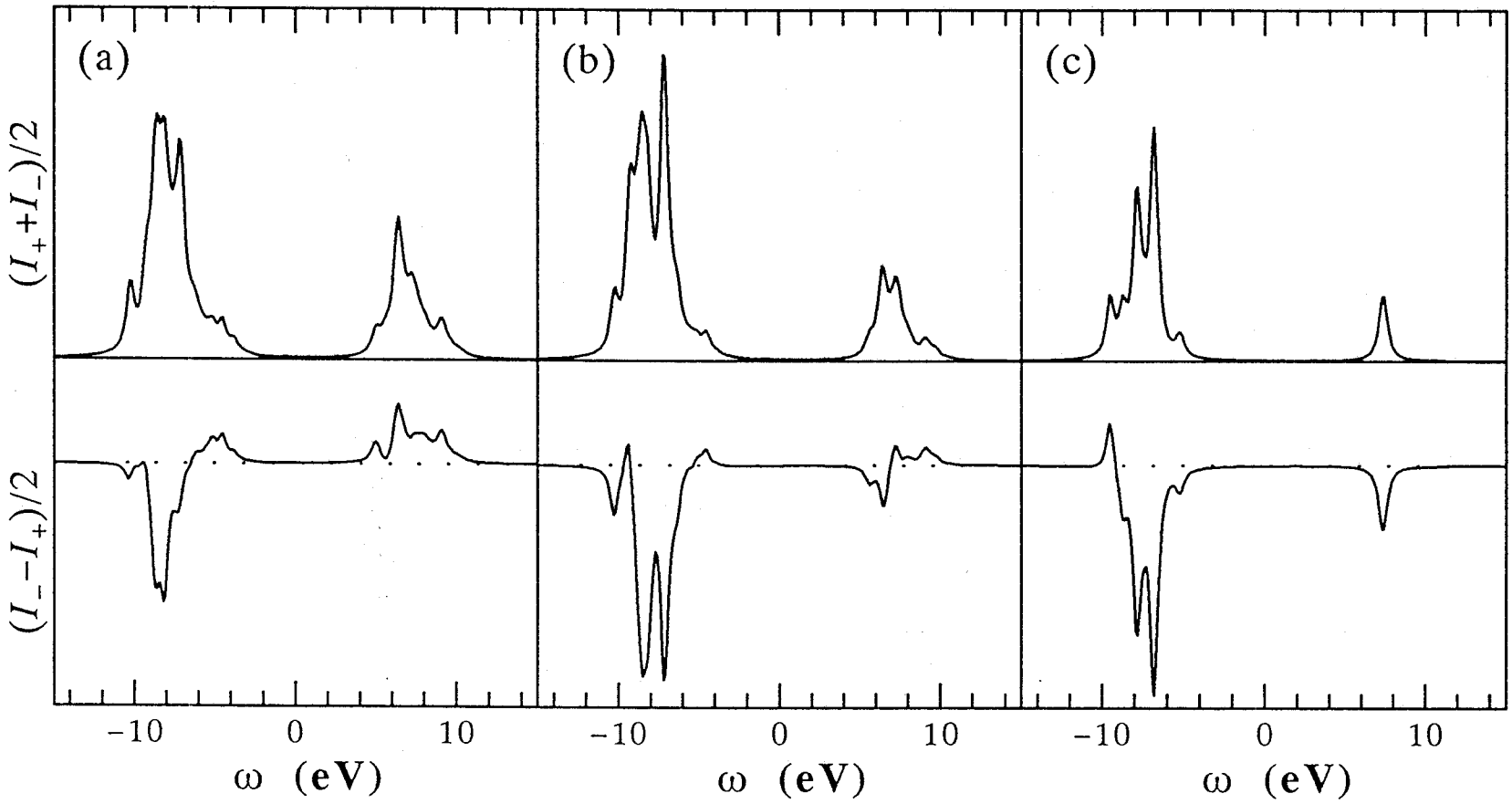

Fig. 4.1. Calculated $2p$ XAS $(I_+ + I_-)/2$ (top) and MCD $(I_- - I_+)/2$ (bottom). (a) Spectra for $10Dq = 1.2$eV and $\zeta_d = 0$ leading $\langle m \rangle = 0$ and $\langle \sigma \rangle = -1.5$. (b) Spectra for $10Dq = 1.2$eV and $\zeta_d = 0.066$eV leading $\langle m \rangle = -1.59$ and $\langle \sigma \rangle = -1.48$. (c) Spectra for $10Dq = 0$ and $\zeta_d = 0.066$eV leading $\langle m \rangle = -3.0$ and $\langle \sigma \rangle = -1.5$. Zero-point of the photon-energy is taken arbitrary.

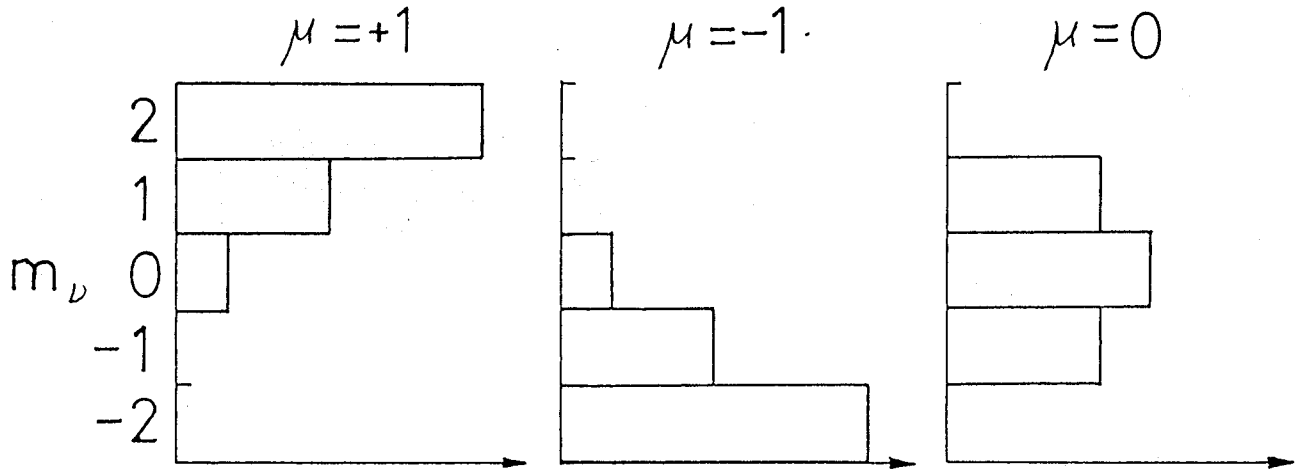

Fig. 4.2. The distribution of $|c^1(2m_\nu, 1\, m_\nu - \mu)|^2$, the weight of the transition to the d state $|\nu\rangle$ in $p \rightarrow d$ photoabsorption by positive helicity($\mu = +1$) and negative helicity($\mu = -1$).

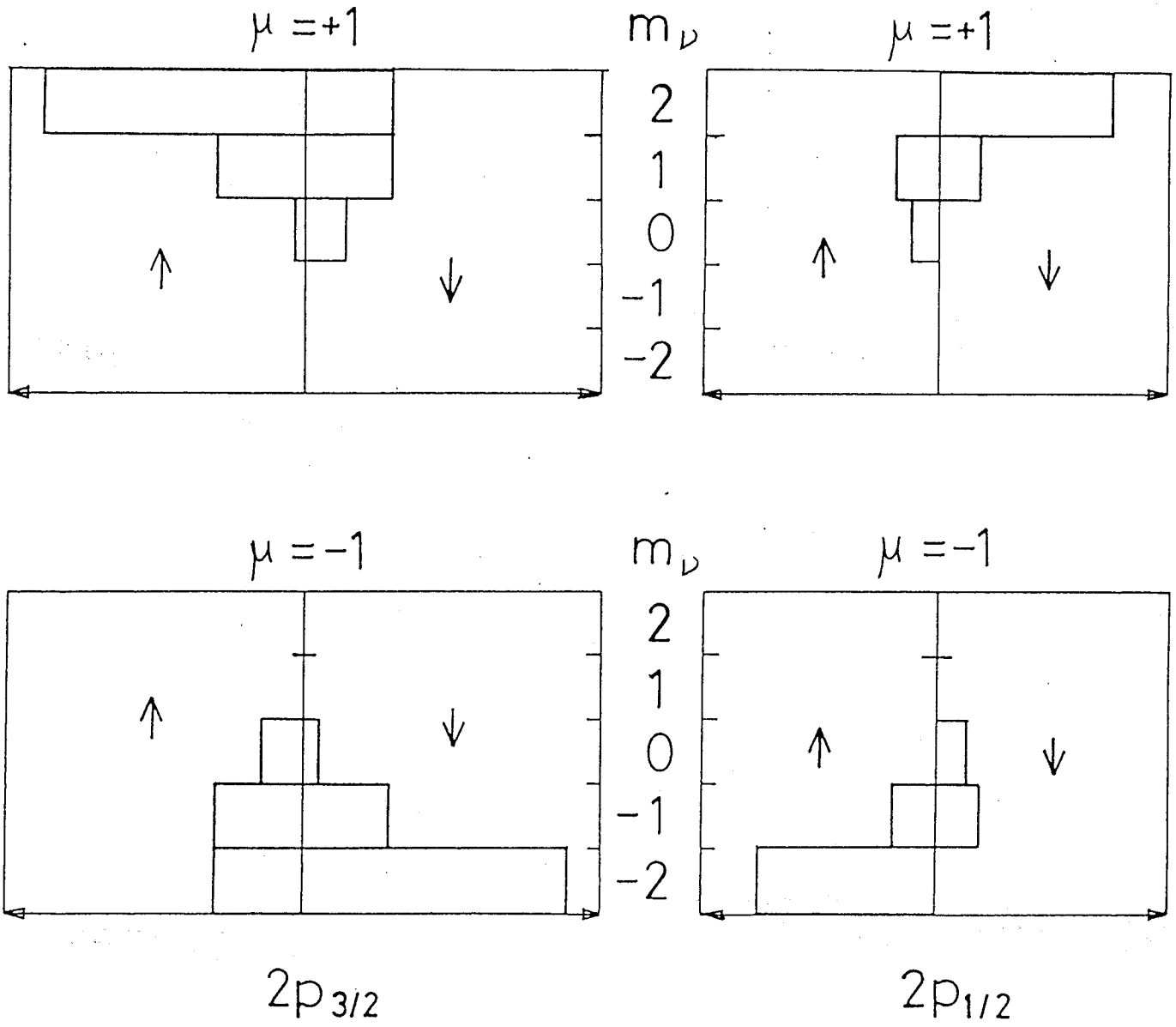

Fig. 4.3. The distribution of the weight of the transition to the d state $|\nu\rangle$ in $p \rightarrow d$ photoabsorption by the light with the polarization μ, when the spin-orbit interaction of the core p hole is strong enough for j of the core hole, which is shown as 'p_j', to be nearly good quantum number.

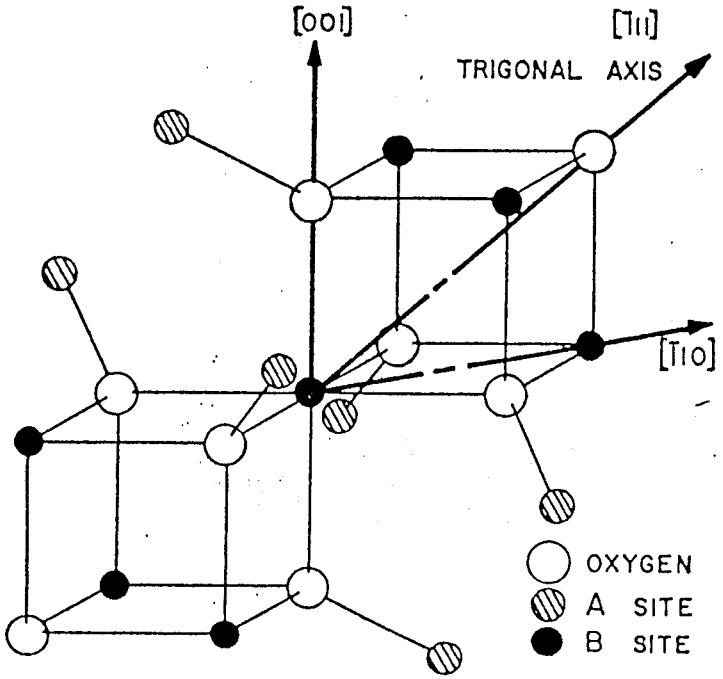

Fig. 4.4. The trigonal symmetry at the B site of the spinel structure.

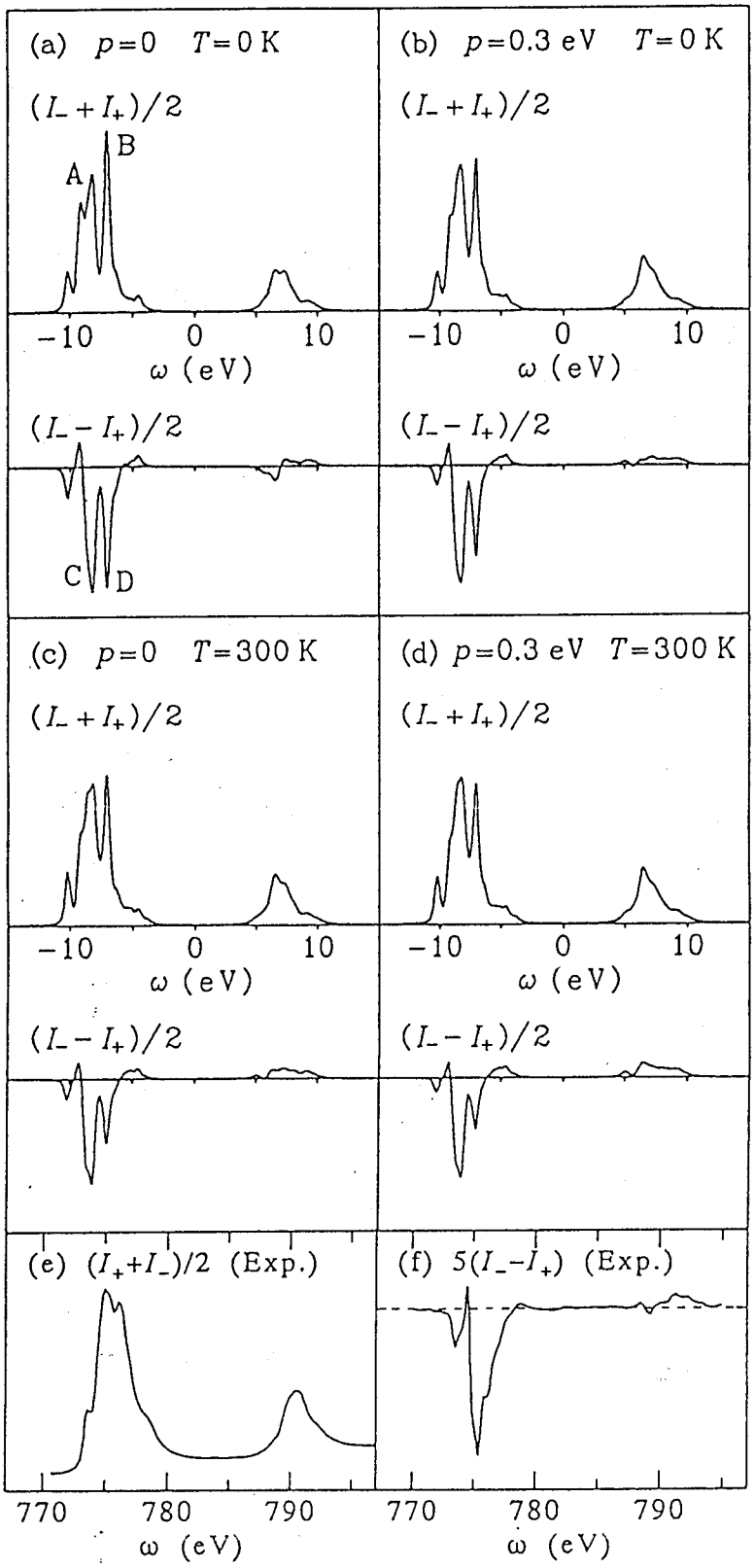

Fig. 4.5 (a)-(d): Calculated total intensity(top) and difference intensity(or MCD: bottom) of $2p$ XAS of magnetic Co^{2+} with X-ray of negative and positive helicity at $T = 0$ and 300 K in octahedral ($p = 0$) and trigonal ($p = 0.3$eV) symmetry(see eq. (4.3)). The effect of the trigonal crystalline field is much more clear in zero-temperature than in room-temperature. Zero-point of the photon-energy is taken arbitrary. (e), (f): Observed total intensity (e) and MCD (f) of $2p$ XAS of Co in a ferrimagnet $CoFe_2O_4$ obtained by Sette at room temperature.[36] These agree well with spectra (c) and (d).

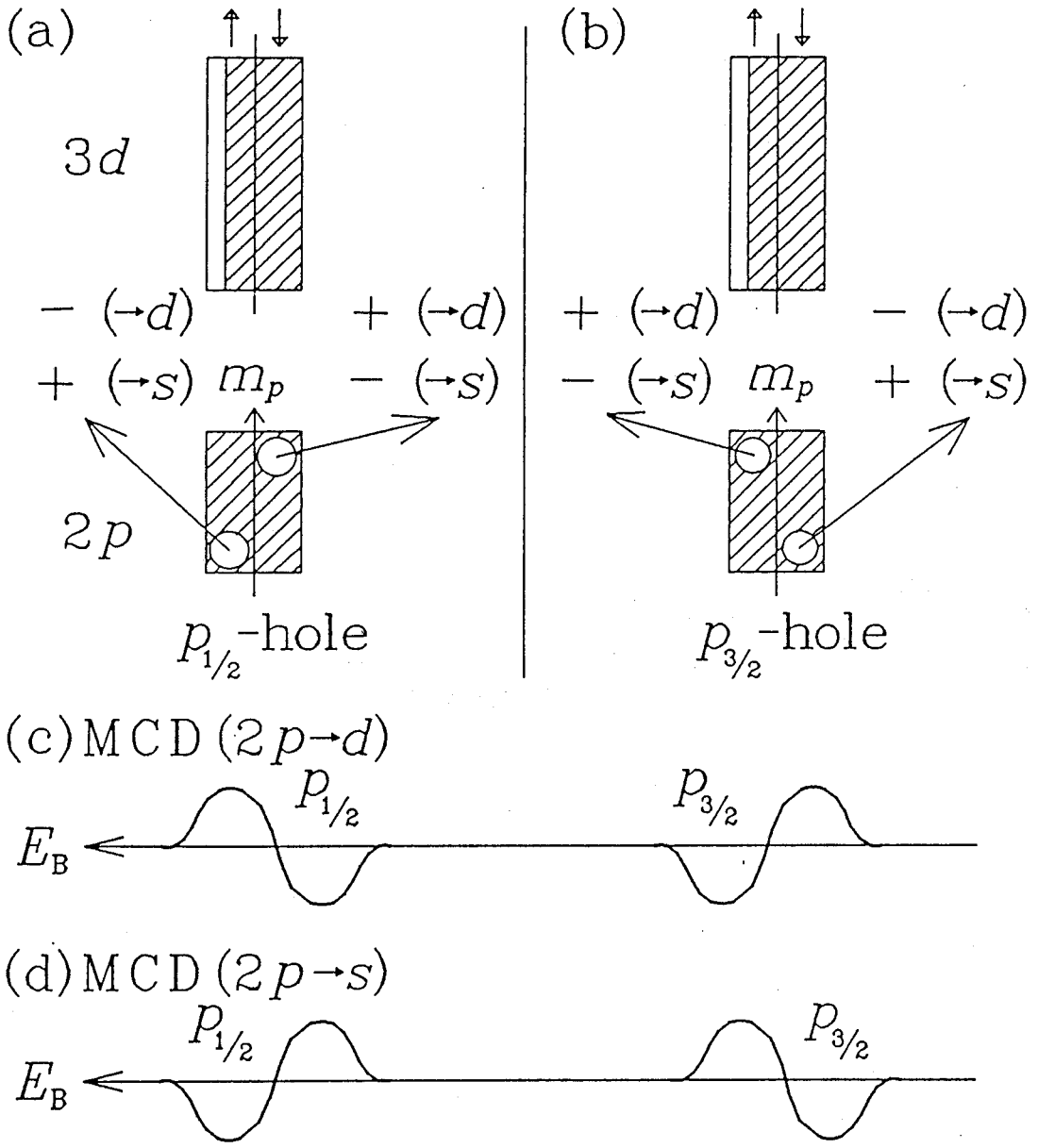

Fig. 5.1 (a), (b): Schematic illustrations of $2p$- and $3d$-hole-distributions (unshaded area) among orbitals specified by azimuthal and spin quantum numbers in the final state of $2p$ XPS for $2p_{1/2}$ (a) and $2p_{3/2}$ (b). '+' and '−' stand for positive and negative helicities respectively. (c), (d): MCD features for $2p \rightarrow d$ (c) and $2p \rightarrow s$ (d) transitions.

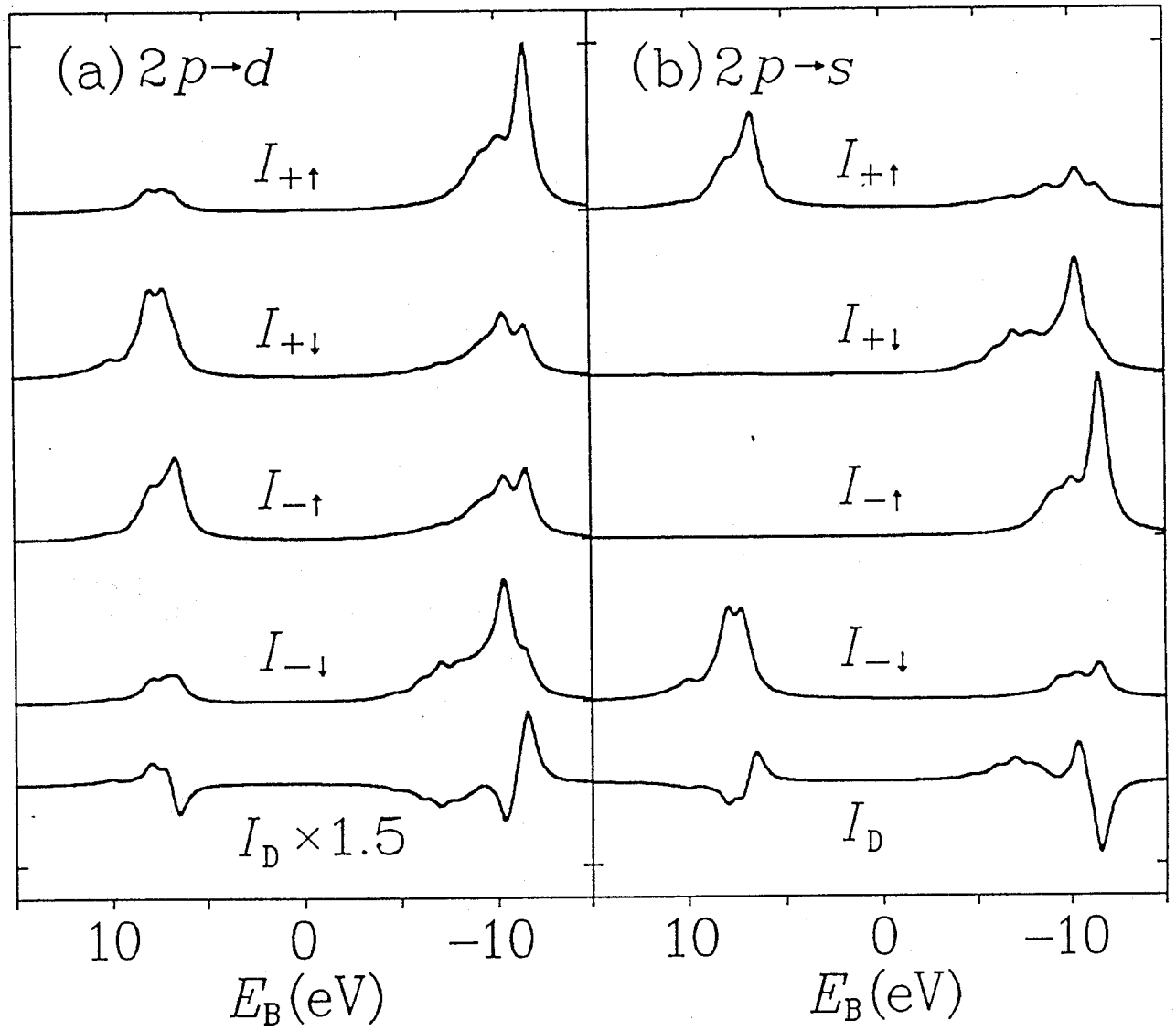

Fig. 5.2 The calculated spectra of $2p \rightarrow d$ (a) and $2p \rightarrow s$ (b) XPS for positive helicity (+) and negative helicity (−) emitting ↑ and ↓ spin photoelectrons and MCD ($I_D = (I_{+\uparrow} + I_{+\downarrow} - I_{-\uparrow} - I_{-\downarrow})/2$). The ground state of $3d^8$ configuration under octahedral cystalline field $10Dq = 1.0eV$ and magnetic field acting on $3d$ spin $\mu_B H = 0.02$ eV with no $3d$ spin-orbit coupling (no orbital moment) is assumed as the initial state.

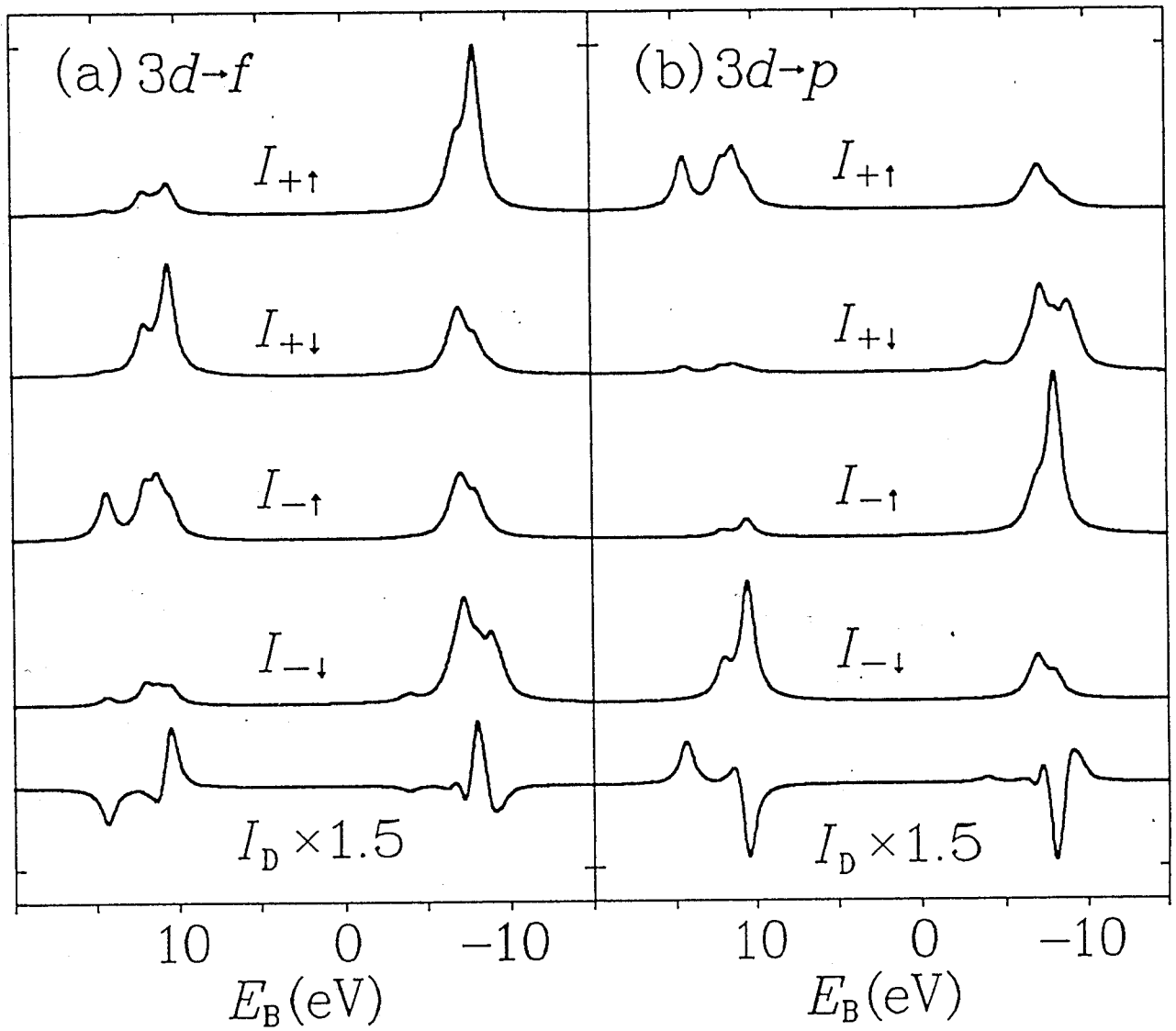

Fig. 5.3 Same as Fig. 5.2 except for $3d \rightarrow f$ (a) and $3d \rightarrow p$ (b) XPS and MCD. The ground state of $4f^1$ configuration under infinitesimal molecular field on the total angular momentum is assumed as the initial state.